Development of a Tandem Microfluidic Two-Phase Extraction Device for Continuous Arylboronic acid Phase-Switching Purification

Paul O'Brien

A Thesis submitted to the Faculty of Graduate Studies in

Partial Fulfillment of the Requirements

for the

Degree of Masters of Science

Graduate Program in Chemistry

York University

North York, Ontario

November 2012

Abstract

The last 20 years has witnessed a surge in the development of fluidic devices and techniques aimed at the generation of novel tools for chemical transformations, chemical analysis, bioassays, therapeutics, medical diagnostics, and in vivo tissue research. A growing area of research involves the use of microfluidics to facilitate reaction optimization and chemical synthesis on a large scale. Although there have been significant gains such as the incorporation of microwave heating, better mass-heat transport, and reduction of impurities through accurate control of reagent addition and reaction parameters, there is a lack of continuous purification techniques to accompany these processes. The development of continuous in-line purification processes is required for the wide scale adoption of continuous flow synthesis. It is necessary since multistep syntheses generally require changing solvents and removal of spent reagents and salts for downstream unit operations or analysis. Developing homogeneous in-line purification processes for flow synthesis would be a boon for industry by enhancing multistep fluidic processes by streamlining unit operations, enabling on demand synthesis of pharmaceuticals for market, resulting in lower costs from storage, spoilage and consignment returns. To achieve this, a method must continuously purify reaction mixtures of salts and by-products for mass spectrometric analysis to produce real-time second by second analysis of flow reactions. We have developed a microfluidic device to perform a tandem extraction process utilizing reversible acid/base phase switching properties of stable arylboronic acids. Using the complexation of boronic acids to 1,3 diol containing sugars, such as glucitol to produce boronic esters with strong hydrogen bonding ability, an aliphatic boronic acid functionalized molecule can be phase transferred from organic to aqueous media and vice versa, to facilitate the removal of impurities under continuous flow conditions. The current project involved the design and optimization of a

simple hybrid device composed of perfluoropolymer film and stainless steel to construct a cheap, easily fabricated and configurable for rapid phase partitioning of boronic acids as a proof of concept methodology for continuous flow purification. Although continuous flow synthesis using fluidic systems has shown promise for single step synthesis, there is considerable difficulty in performing sequential steps to build complex small molecules. However, with the development of a continuous flow purification method this may be ameliorated so that a general method of multistep synthesis can be developed. The use of extraction techniques to facilitate purifications in continuous flow systems may prove to be a reliable and sustainable method for small scale as well as industrial scale synthesis as opposed to the use of liquid chromatography of intermediates, which introduces greater unit operations, steps and exponentially increases costs of APIs. Although the current project was not successful in generating a fully optimized device with a total arylboronic acid recovery of ~95%, we did achieve a high recovery of 75%. The proof of concept device demonstrated the utility and promise this system holds for developing multistep inline synthesis and analysis in-flow but requires further work to fabricate a more suitable microfluidic device to conduct arylboronic acid phase-switching purifications.

Acknowledgements

I would like to thank my supervisor Dr. Michael G. Organ for his advice, support and trust during my stay with his research group. Beginning my MSc was daunting since my project was largely outside of my previous academic studies but the combination of Dr. Organs enthusiasm and Dr. Derek Wilsons experience in microfluidics helped me push through initial setbacks to accomplish project milestones. During my MSc I was not only exposed to microfluidics and various fabrication techniques but also advanced organic and organometallic chemistry, where Dr. Organ pushed me to have a greater understanding chemistry fundamentals, which has proven to be invaluable in my subsequent studies.

I wish to thank my supervisory committee for their support, imparted knowledge and time expended to correct and critique my thesis. I want to thank Dr. Wilson for his informative talks concerning the fine details of practical microfluidic applications and fabrication. His help and knowledge helped me to expand, appreciate and further pursue microfluidics in the larger field of science. I would also like to thank Dr. Arturo Orellana for spending his time aiding and deepening my knowledge of organic chemistry and problem solving skills, through his courses and weekly organic problem sessions. These sessions greatly expanded my understanding and critical analysis of organic reaction mechanisms, which will be a significant aid in the pursuit of my career in science.

I would like to thank my family for their support, while instilling in me from a young age the work ethic to pursue my ambitions, their care and love has carried me far on my travels in life.

I also wish to thank all of my colleagues from the Chemistry department, whom have made my stay a great experience, while the friendships I have made here will hopefully be

lifelong. They have not only given their friendship but also guidance and support through difficult times.

Table of Contents

List of Tables

List of Figures

List of Abbreviations

∇ Del operator

∇^2 Laplace operator

θ contact angle of a liquid with a solid surface

DIBAL-H diisobutylaluminium hydride

D diffusion coefficient

DMSO dimethyl sulfoxide

EtOAc ethyl acetate

h microchannel characteristic micron-sized dimension

LIGA lithographie, galvanoformung, abformung

MS mass spectrometry

η dynamic fluid viscosity

n_x, n_y aspect ratio of channel (height/ width)

Δp relative pressure difference (backpressure)

P partition coefficient

p absolute pressure

ρ fluid density

p* absolute fluid outlet pressure

p(0) absolute fluid inlet pressure

pBA p-tolylboronic acid

p_b break-through pressure (pressure once reached a particular fluid will flow through the channel)

p_c capillary pressure

PDMS polydimethylsiloxane

PEE poly ethyl ether

PEEK polyetheretherketone

PMMA poly methylmethacrylate

PTFE polytetrafluoroethylene

Re dimensionless Reynolds number

SAMs self-assembled monolayers

t time

v flow velocity

v kinematic viscosity

v_{max} maximum channel flow velocity

V_o mean fluid velocity

v(x,y) point velocity

x travel distance of a particle

x, y distance values between –X to X and –Y to Y channel walls

X, Y center point distance to channel wall

γ interfacial tension between the two fluids

Chapter 1

1.0 Introduction

1.1 Microfluidic Devices

The advancement of chemistry in industrial and academic laboratories over the last 200 years has been dominated by the use of vessel reactors, ranging in capacity from a few milliliters to hundreds of liters. However, future developments require novel methodologies such as microfluidics for greater understanding of fast reaction kinetics, thermodynamics and reaction mechanisms to allow new synthetic methodologies previously believed to be inaccessible. In this regard, microfluidic devices are poised to shift traditional methods of batch chemical synthesis towards the use of flow devices utilizing microliter reactor volumes. This technology has the potential to revolutionize chemical synthesis by increasing energy efficiency, producing cleaner reaction products, environmentally sustainable methodologies and safer synthesis using hazardous chemical intermediates.

There are 3 main classes of flow devices of arbitrary cross-sectional shape (Figure 1). The first type of flow device (Figure 1A) incorporates either micro or meso scale channels with solid supported materials, that interact with the mobile phase such as a variety of reactants, reagents or catalysts.[1]

Figure 1: Depiction of different types of fluidic channels from left to right; A) solid supported channels with reagent covalently bonded to channel surface; B) microfluidic channel with diameter of less than 500um; C) meso-fluidic channel between 1mm-500um.

Larger reactor sizes between 500μm and 1mm are referred to as mesofluidic channels (Figure 1B). The smallest devices are called microfluidic channels, and are characterized by having a cross-sectional dimension of less than 500 micrometers (Figure 1C). Flow reactors are typically characterized as a closed system with a tube-like design, where a fluid passes through the reactor space and exits the system after a well-defined period of time, referred to as residence time. Flow channels have been incorporated into complex flow networks with integrated unit operations such as multiple sequential operations, purification steps, or analysis before exiting the device.

Continuous flow reactors are designed to accept a constant infusion of material into a microsized reactor volume where unit operations are performed as the reaction fluid travels through the microspace while the product is collected continuously. With the constant influx of reactants, microliter flow reactors can compete with larger vessels for production of material, thorough 'scaling out' production, defined as the use of parallel flow channels to increase production, while vessel reactors 'scale up' preparation of more material by using larger volumes. There are a number of advantages that make the adoption of continuous flow devices attractive to industry, such as the elimination of scale up optimization, saving labour, time and cost since scaled-out microfluidic reactors operate under identical conditions, while scaled up reactions

typically do not operate under the same conditions at smaller scales. Microsized continuous flow reactors have advantages over stirred tank reactors, such as decreased mixing time, better uniform temperature control, larger surface to volume ratios, precise residence time control and spatial separation of reactants and products.[2] Recently, flow chemistry has become attractive to industry because of the concept of 'on demand' synthesis. Since pharmaceutical products are on consignment to pharmacies, have a one year shelf-live and requires constant quality control while in storage waiting for purchase, on demand synthesis would eliminate storage, quality control and spoilage costs by adopting 'just in time' manufacturing techniques offered by flow chemistry.

Roberge has described how different classes of transformations benefit from microfluidic techniques based upon their kinetics; Type A are instantaneous reactions with half-lives ($t_{1/2}$) of $t_{1/2} < 1s$, Type B are fast reactions $1s < t_{1/2} < 10min$, and Type C are slow reactions with $t_{1/2} > 10min$.[3] Type A benefits from a flow approach to synthesis because these processes are controlled by mixing, since the reaction mainly takes place in the micromixing zone, the type of mixer and the flow rate play a significant role in reaction outcome. Type B reactions are kinetically controlled and therefore require low temperatures and small temperature gradients to produce clean products, therefore microstructured channels are beneficial since they display lower temperature gradients than large scale techniques and have better mixing from higher surface area contact of phases. Finally, Type C reaction kinetics are too slow to directly benefit from microspace reactors, but highly exothermic reactions and autocatalytic processes benefit by reducing the amount of unstable or explosive intermediate produced at any one time coupled with fast heat dissipation from high surface-volume ratios.

Microfluidic flow reactors also provide advantages for chemical transformations because of the spatial and temporal separation of infused starting material from the transformed product

through the length of the channel. This can potentially produce cleaner reaction products since products do not reside under harsh reaction conditions for extended periods of time but are eluted and quenched quickly after the transformation has taken place. The decreased exposure of individual molecules to high temperature and excess reagents reduce the chance of decomposition or side reactions.

The small size of microreactors translates to better heat and mass transfer due to greater surface area contact between fluids and reactor surfaces. The increase in mass transfer or mixing not only benefits Type A reactions but also aids in the fast production of small quantities of material. By decreasing reaction times of small quantities of products, iterative optimization reactions and analysis can be performed faster with higher efficiency and moved into scale out conditions to bring a product to market in a much shorter time frame.

Although there are many potential benefits from the incorporation of microfluidic devices into chemical production, there are some experimental design considerations that must be evaluated on a case by case basis. A major drawback stems from the blockage of microchannels due to particulate formation and aggregation. This problem is magnified when microfluidics are employed for heterogeneous applications. Therefore any process performed must be homogeneous from initiation to termination to avoid channel blockages. Even with homogeneous microfluidic transformations, shear-induced crystallization[4] is a known phenomenon, although the mechanisms for crystal growth are currently unclear. This can be solved in some situations with the use of targeted microwave heating or localized sonication to break up or inhibit crystal growth. Remarkably this phenomenon has been successfully employed for nanocrystal production using microfluidic devices.[5] Some disadvantages arise from the presence of laminar

flow, where dispersion of analyte occurs along the axis of flow, which is attributed to the parabolic velocity profile (Figure 2).

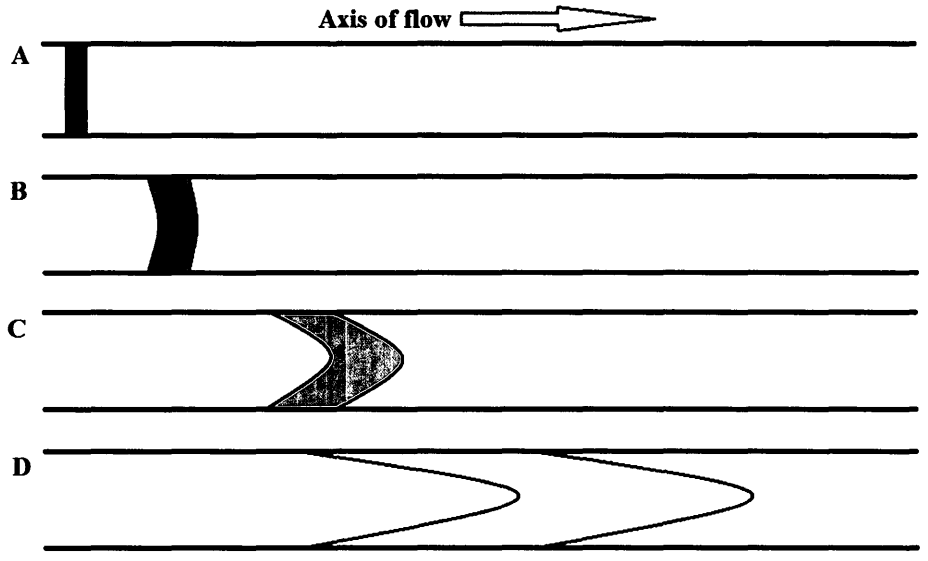

Figure 2: Depiction of an analyte injected into a microfluidic tube of arbitrary cross-section resulting in band broadening under laminar flow conditions. (A) concentrated analyte injected into the reactor. (B) initial flow of analyte that begins to disperse according to the flow profile. (C) as flow time lengthens the dispersion becomes more pronounced due to slow flow close to the channel walls. (D) axial dispersion of the analyte becomes more pronounced over time leading to greatly lengthened elution times of the analyte or band broadening that resembles the flow velocity profile.

The problem of band broadening is compounded by the lack of turbulent mixing under laminar flow conditions, resulting in poor mixing of miscible fluids in microfluidic chambers. This is caused by the strong interaction of the tube walls with the fluid surface which induces a highly ordered flow where turbulence is suppressed, resulting in much longer reaction times with mixing occurring by diffusion only. Some groups have improved mixing under laminar conditions by using pulse flow or oscillating flow, where flow has a periodic forward and reversal motion which promotes turbulent mixing in the microchannel. While microfluidics is an emerging technique for performing different unit operations with increasing complexity it is challenging to build and implement complex networks since theoretical frameworks rarely model fluid

behaviour accurately, resulting in poor overall device performance or unstable flow behaviour over time.

Many reactor designs have been fabricated and tested in an attempt to address these issues but some of the largest hurdles facing the adoption of microreactors for industrial and academic applications remain. As such, the fabrication and scale up of flow reactors for commercial use remains an elusive goal.

1.2 Fabrication of Teflon-Steel Hybrid Microfluidic Device

Fabrication techniques of microfluidic devices were initially borrowed from the semiconductor microprocessor industry, where techniques for reliably reproducing small structures on silicon substrates are well known. Initial microfluidic devices were developed from silicon and incorporated into analytical technologies such as integrated microfluidic gas chromatography columns.[6] While this initially benefited analytical chemists, incremental improvements in materials used, design, and creativity allowed microfluidic devices to branch out into organic chemistry,[7] biology,[8] pharmacology,[9] therapeutics,[10] and medical diagnostics.[11,12] The advent of new fabrication technologies, such as stereolithography,[13] laser ablation,[14,15] and manipulations of microfluidic flows to form small internal structures in channel surfaces,[16] has resulted in an increase in the number of new microchannel designs. These novel designs have led to significant advancements in chemical analysis,[17] engineering,[18] chemical kinetics, medicine[19] and enzymatic kinetics.[20]

Microfluidics can be adapted to a vast array of applications, which necessitates construction from different materials such as stainless steel, elastomers, silicon, glass or hybrid materials (Figure 3). Different materials impart advantages to overcome specific hurdles in

microfluidic applications such as robustness, solvent sensitivity, gas permeability, high pressures, unit cost, technical fabrication problems, and high aspect ratio (height/width) microstructure fabrication. However, the design and production of microfluidic devices from standard materials is a lingering issue. Difficulties are especially pronounced for steel, silicon and glass devices that require expensive infrastructure and technical skills for production.[21,22]

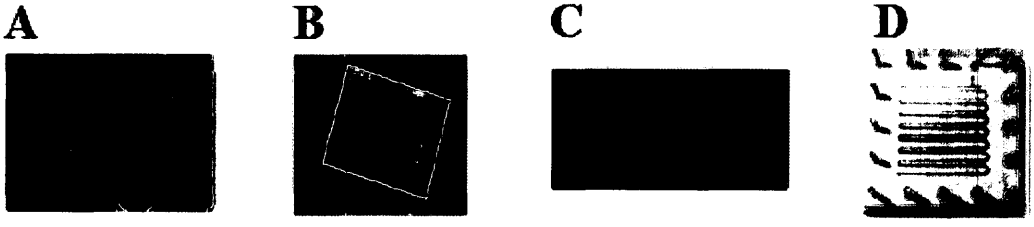

Figure 3: Different material types of developed microreactors (A) Steel microreactor, (B) Silicon microreactor, (C) glass microreactor, (D) Hybrid steel and Teflon ® microreactor

Also, irreversible bonding processes employed in the production of microchannels limit the usability of microfluidic chips once clogged. The production of microfluidic steel structures using lithographie, galvanoformung, abformung (LIGA) processes[23,24] are expensive and technically difficult to reliably fabricate, which severely limits adoption. The expense of producing microstructures in silicon, glass and metal-based substrates has created a need in industry and academia to produce new fabrication techniques and materials for microfluidic devices, leading to the development of novel elastomer materials and manufacturing methods.

Elastomeric microfluidic devices use polymer substrates such as poly (dimethylsiloxane) (PDMS), poly (methyl methacrylate) (PMMA), poly (ethyl ether) (PEE), polycarbonate, and fluorous polymers, such as poly (tetrafluoroethylene) (PTFE) for the formation of microstructures. Polymers offer excellent mechanical properties and produce quality low aspect ratio structures through soft lithographic techniques such as, imprinting, and hot embossing,[25]

While non-fluorinated polymer devices can be fabricated using soft lithographic techniques, such as injection moulding, they suffer from the inability to tolerate harsh organic solvents, which cause decomposition, swelling, or dissolution. Whereas fluorinated elastomer materials are resistant to harsh solvents, strong acids, and bases, making these materials very attractive as fluidic reactor materials. Hence PTFE materials offer a cost effective means to prepare microfluidic devices which utilize harsh conditions.

Fabrication of PTFE microstructures is largely limited to the use of laser ablation techniques. In laser ablation a directed laser beam is used to locally heat and vaporize/remove material from the surface, leaving a depression that is proportional to the energy of the beam. When a beam is drawn across the surface, a trough with a parabolic profile is made, reflecting the Gaussian energy distribution of the laser beam profile. A Guassian distribution best describes a laser beam cross-section, where the most intense energy is located in the center of the beam and the energy intensity decays as the distance from the center increases, and is translated into the surface topology of the cut. Ablation is a beneficial method since control of laser power allows the engraving of shallow channels, in conjunction with cutting through the entirety of the material if desired.[26]

The use of laser ablation for engraving PTFE, coupled with pressure sealing machined steel chucks, creates hybrid reactors that are robust and functional compared to tradition glass or silicon devices. Hybrid reactors are composed of a gasket material where the negative space is the fluid channel, and the chuck forms the top and bottom of the channel with the fluidic ports embedded in the chuck material (Figure 4). Hybrid reactor designs offer ease of fabrication, material durability, chemical resistance, tolerance to high back pressures and modular

functionality as advantages. Hence, hybrid fluidic reactors have proved successful in industry and academia for the synthesis of nanoparticles and multiphase flow applications. [27,28]

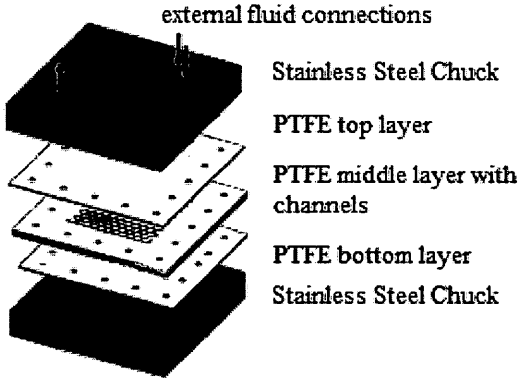

Figure 4: Teflon gasket Hybrid fluidic device, incorporating PTFE lining, piezoelectric actuation (sonication), and heating element, *Jensen et al.*

These designs have the added benefit of easy incorporation of additional elements such as heating/cooling, and sonication (Figure 4) through insertion of compressible elements between layers.

1.3 Fluid Transport in Microchannels

Mass-transport through microchannels is critical to the design and implementation of microfluidic devices, where methods for pumping fluids fall under two broad categories: dynamic pumping and displacement pumping. Dynamic pumping refers to the creation of high fluid velocities and subsequent conversion of velocity to pressure by axial dispersion through the channel, while displacement pumping refers to the use of physical means to displace or push fluid using a pressure differential between the fluid source and fluid destination. Dynamic pumping has been exploited for direct integration into microfluidic devices, using centrifugal,[29] electrohydrodynamic,[30] electroosmotic,[31] acoustic streaming,[32] surface-tension induced flow,[33]

and electrowetting techniques.[34] This method benefits small footprint devices[35,36] by providing an internal pump but typically operate at low flow rates and ultra-low sample volumes making these methods incapable of sustaining continuous high throughput flow applications.[37] Displacement or pressure-driven flow (Figure 5) involves the formation of a pressure difference Δp between input pressure p(0) of reagents and outlet product pressure p*.

Figure 5: Diagram showing pressure driven flow inside of a microchannel; p(0) is the total pressure generated by the displacement pump, p* is atmospheric pressure, Δp is the backpressure generated by the liquid resisting flow through the length (L) of the microchannel.

A piston generates positive pressure p(0) by fluid compression and relieved by flow to an area of lower pressure (p*), this involves using syringe pumps to create pressure in the flow network, while the outlet is open to atmospheric pressure. Displacement pumping offers the advantage of robust, simple and continuous pumping, through the use of multiple cycling pumps, peristaltic pumps or air actuated pumping. The coupling of pumps to fluidic devices is largely accomplished through the use of Luer-lock technology, which makes use of high pressure fittings and connections between tubing and other components. This technology minimizes the potential for leaks generated from high back pressure systems (Δp) without the aid of special tools.

Back pressure arises in pressure-driven systems stemming from flow rate, channel cross-section area, channel length and fluid viscosity. The relationship between fluid, channel area cross-sectional area, flow rate and viscosity are modelled by a solution to the Hagen-Poiseuille equation (Equation 1),[38] where v is the average linear velocity, μ is the kinematic viscosity, L is channel length, h is the height, w is the width, and ΔP is the pressure drop across the two ends of

the channel. This equation takes into account the development of the velocity profile along the length of the microchannel, using an experimentally determined constant. Poiseuille equations are a class of analytical solutions derived from the Navier-Stokes equation (Equation 2)[39] which apply to pressure-driven steady-state flow conditions in microchannels where v is the flow velocity, ρ is the fluid density, p is the pressure, ∇^2 is the Laplace operator, ∇ is the del operator and *Re* is the dimensionless Reynolds number.

$$\Delta P = \frac{12v\mu L}{h^3 w\left(1 - 0.63\left(\frac{h}{w}\right)\right)} \qquad (1)$$

$$\frac{\partial}{\partial_t}\vec{v} = -\nabla p + \frac{1}{\mathrm{Re}}\nabla^2\vec{v} \qquad (2)$$

The Navier-Stokes equation uses non-dimensional values to describe fluid flow, where *Re* numbers of Re<<1, the viscosity term ($\nabla^2 v$) dominates but as Re>>1 then the inertia term ($v \cdot \nabla$) dominates. Reynolds Number (Re) is an important parameter of fluidic systems because it predicts how mixing occurs within the channel, where there is a transition from laminar flow to turbulent flow around 2300Re, which indicates a transition from diffusion only mixing to chaotic mixing.

Channel geometry has a large impact upon the velocity profile of fluids travelling through a microchannel. The velocity profile arises from the interaction of the fluid with the side walls of the channel producing disproportional shear forces across the internal volume of the microspace, which slows the fluid near the channel walls and becomes progressively faster towards the center of the channel. The channel geometry effects the profile shape (Figure 6), where a circular

channel is radially symmetrical leading to a symmetrical conical profile shape (Figure 6A). Conversely a square shaped microchannel is not radially symmetrical and produces a square-like velocity profile (Figure 6B).[40] Laminar flow can be predicted using Reynolds number (*Re*). Reynolds number is a dimensionless number that represents the ratio of inertial to viscous forces acting in a flowing liquid where ρ is the density of the fluid, V_o is the mean velocity of the fluid, η is the dynamic viscosity, and h represents the microchannel characteristic dimension, shown in (Equation 3).[41]

$$\mathrm{Re} = \frac{\rho V_o h}{\eta} \quad (3)$$

The velocity profile of common square channels used in chip based microfluidics (Figure 6B) can be found using (Eq 4), where the real velocity at a point in the channel v(x,y) can be found using the maximum flow velocity v_{max} located at the center of the channel, X and Y are the distance from the center point of the channel to the respective side wall, x and y are distance values that are between –X to X and –Y to Y, while n_x and n_y are calculated using the aspect ratio of the respective channel.[42] This approximation of the parabolic profile in a square channel closely resembles the profile generated in circular tubes but it introduces ~5% error, unless the exact solutions are utilized. This equation applies to most square channel designs and is particularly useful in describing extraction or dilution in two similar solvents for analytical purposes.

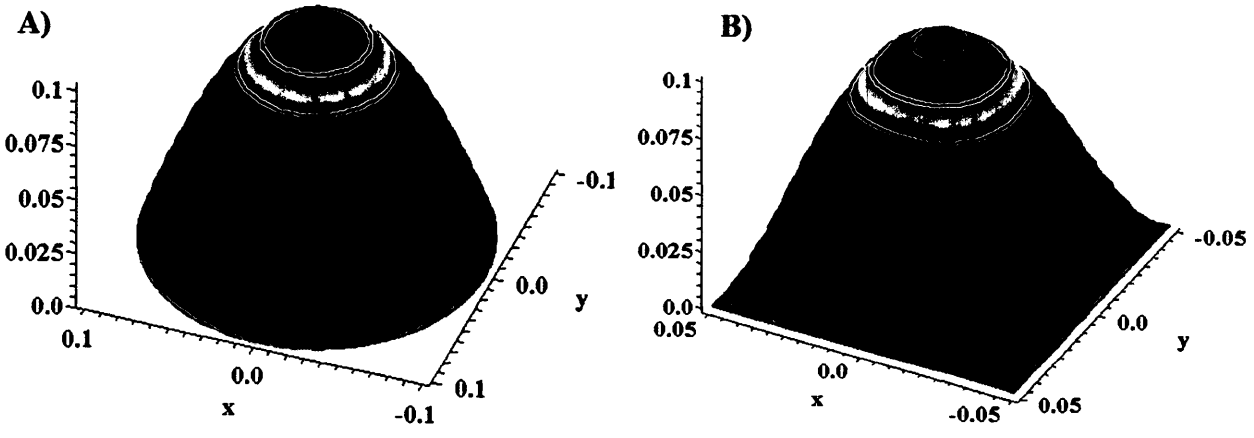

Figure 6: Cartesian (x,y,z) coordinate graphs depicting the flow velocity profile of pressure driven flows in microchannels. A) flow velocity profile through a circular tube. B) flow velocity profile through a square channel[43].

$$v(x,y) = v_{max}\left(1-\left(\frac{|x|}{X}\right)^{n_x}\right)\left(1-\left(\frac{|y|}{Y}\right)^{n_y}\right) \qquad (4)$$

1.4 Laminar Flow in Simple Microchannels

Microscale flow reactors operating under pressure-driven flow can produce a phenomenon called laminar flow under certain flow regimes. Laminar flow produces an organized parabolic cross-sectional velocity profile resulting from the friction of the fluid-solid boundary layer molecules which adhere to the surface of the microchannel and slow the adjacent layers of fluid. This results in the formation of parallel planes of increasing velocity towards the center of the flow, shown in (Figure 4), where the arrows represent vector velocities.

Renoylds number (Equation 3) can be accurately estimated under specific flow conditions, where laminar flow is favoured (Re < 2300) or turbulent flow is favoured (Re > 2300). The viscous term (η) promotes laminar flow because of fluid organization with the channel walls while the inertial term ($\rho V_o h$) promotes turbulent flow through chaotic motion

generated from the inertia of the fluid. There is no clear transition barrier between laminar flow and turbulent but rather a gradient as laminar flow becomes weaker and transitions to turbulent flow as *Re* approaches 2300.

Reynolds number is important because it differentiates between laminar flow and turbulent flow behaviour in a microchannel, where the ordered fluid under laminar flow conditions will only mix through diffusion. This is a major concern since diffusion is slower than turbulent mixing methods, but on very small length scales diffusion can become faster than turbulent mixing. A simple calculation (Equation 4), where x is the characteristic diffusion distance perpendicular to the direction of flow, D is the diffusion coefficient for a particular particle or molecule, and t is time required for the movement of a particle to move across x, demonstrates that mixing is faster at smaller length scales.

$$t_{diff} = \frac{\left(\frac{2}{3}x\right)^2}{D} \qquad (4)$$

This formula (Equation 4) indicates the speed of mixing two contacted fluids is enhanced as the reaction channel becomes smaller, resulting in decreased time for complete mixing to occur.

1.5 Two-Phase Microfluidics

Two-phase flows are generated using immiscible fluids, such as gas-liquid, liquid-liquid or supercritical fluids, where the paired phases are not soluble in one another. The utilization of two phase microfluidic devices is a popular method for reactions, extractions, analysis and formation of molecular and colloidal micelles. There are three general types of two phase laminar flow that develop inside microchannels using different techniques and channel designs;

stratified, countercurrent and segmented flow. As two streams of immiscible fluids contact one another, the streams undergo an arrangement that takes place within a few micrometers of contact into the most stable configuration based upon prevailing fluidic conditions.

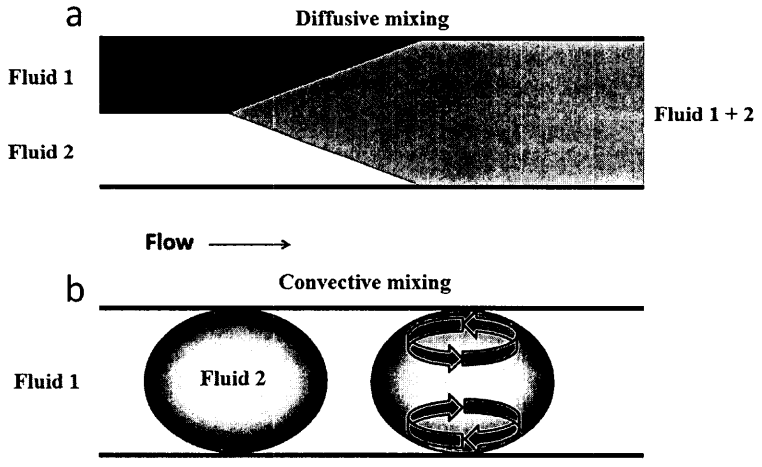

Figure 7: depiction of a) diffusive mixing of two contacted fluid streams and b) convective mixing within droplets due to drag caused by close proximity of droplet surface to the channel wall.

Stratified two-phase laminar flow is a common regime used in fluidic devices, involving coaxial flow of material through microchannels where the interface of the two fluids extends the length of the channel and the stability of the interface is based upon the superficial flow rate, inlet geometries and surface wetting properties (Figure 7a). Increased instability causes the streams to break up into droplets, which is a more stable configuration for immiscible flows to adopt, based upon lower surface energies of droplets in a moving phase. Stratified flows are usually stabilized by the selective wetting of surfaces on the channel walls, pillar structures placed along the interface, or surfactants. Selective wetting surfaces stabilize the elongated interface of aqueous-organic biphasic flows by promoting the organic wetting of one side of the channel with hydrophobic groups, typically long chain alkyl groups, while the other side maintains the hydrophilic wetting of glass. Kim *et al.* used surface patterning in the form of self-assembled

monolayers (SAMs) using flow techniques to react octadecyl-tri-chloro-silane with glass surfaces to produce selective organic wetting.[44]

Countercurrent laminar flow refers to two phases contacting and flowing in opposing directions along the same axis. Kitamori used this technique to increase extraction efficiency of simple organic-aqueous extractions, which increased the theoretical plate height of their microfluidic reactor. Plate height refers to establishing a zone where an equilibrium process occurs, meaning increased plate height results in higher separation efficiency in a smaller area. Kitamori was able to achieve a theoretical plate height of 4.6, while stratified extraction can only achieve a maximum plate height of 1.[45] The use of countercurrent flow is severely limited due to ultra-low flow rates, but most importantly, chemically modified surfaces (SAMs) rapidly degrade through steady erosion or engulfment by the bulk material, resulting in the loss of the desired selective wetting properties.

Lastly, segmented flow involves the generation of droplets of fluid within a moving stream (Figure 7b), which form as a result of flow instabilities that disrupt the interface. The generation of flow instabilities that result in segmented flow is an active area of research where a variety of techniques have been developed to produce highly periodic bubble flows of known diameter with a narrow size distribution. Bubble flows typically develop from flow instabilities in confined microchannels through capillary instabilities,[46,47] pressure-drop induced breakup[48] and Kelvin-Helmholtz instabilities.[49] The development of reliable and fast methods for the generation of emulsions with low polydispersity is important since droplet flows reduce or eliminate axial dispersion of reagents (Figure 8), while allowing faster mixing within droplets due convection and higher surface area contact with the moving phase.

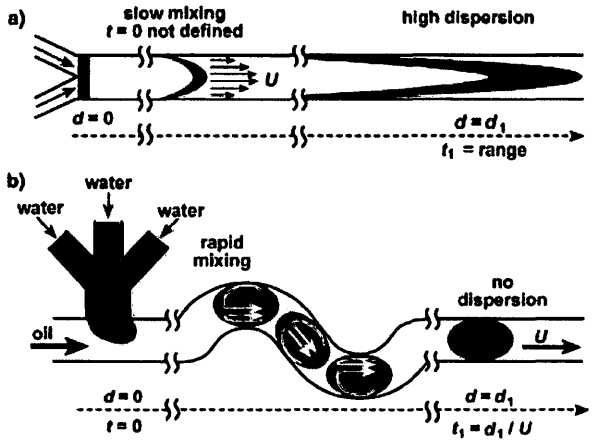

Figure 8: Depiction of stratified laminar flow mixing a) versus mixing using droplets b). Stratified laminar flow a) results in high axial dispersion of the reagents through the channel, while droplets separated by an inert carrier b) result in rapid mixing through circulation within the droplet and no reagent dispersion due to encapsulation.[50]

Many groups have developed their own methods for the introduction of passive and active microreactor mixers, such as three dimensional serpentine channels,[51] emulsions,[52] and coalescence mixers.[53] By contacting immiscible phases in microchannels, the partitioning of species results in crude purifications that are much faster than hand shaking separatory funnel techniques due to increased surface to volume ratio. This continuous separation of phases can be coupled to subsequent reaction steps, collected, or sent for analysis in much shorter time frames.

1.6 Microfluidic Separation of Phases

The separation of immiscible phases has traditionally been carried out using settling, where fluids partition from one another according their density, which are then siphoned off at strategically placed outlets (Figure 9). Gravity separation is an effective method for large scale batch reactions and workup where biphasic systems remain in contact for extended periods of time.

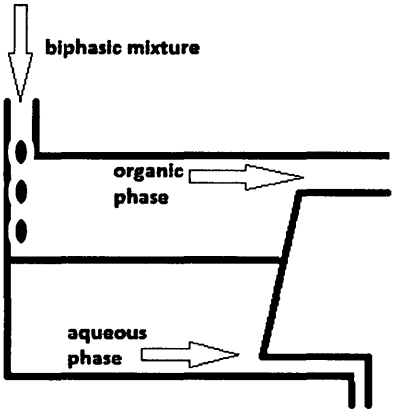

Figure 9: Schematic of phase separation using the tank settling (settling pond) technique: separation occurs when the immiscible phase of higher density settles to the bottom of tank and in siphoned away, while the lighter phase is removed from the top of the tank.

Consequently, the development of fast microfluidic extractions and subsequent separation of phases has led to novel techniques which can potentially reduce lost product from side reactions and enable fast on-demand analysis of unit operation outcomes. Devices for microfluidic separations of molecular or particulate species have been recently developed for cell separators,[54] blood dialysis,[55] nanoparticle separation,[56] metal extractors,[57] chemical extractor[58] and two-phase chemical reactors.[59]

To optimize the separation of two-phase flows to produce two relatively uncontaminated phases, a plethora of solutions have been developed. To separate phases, groups have developed strategies that include inducing stratified laminar flow using surface modification for selective wetting,[60] membranes,[61] pillars,[62,63] limiting channel design and capillary designs[64] to afford phase separation by directing different phases to spatially separated outlet ports. These modifications produce the effect of controlling the path of the liquids so precise contact is made but the phases are selectively directed towards different outlets.

The use of selective surface wetting has been used by numerous groups to stabilize two phase aqueous-organic flows. This technique typically involves the treatment of glass channels with alkylsilyl based SAMs. The alkylsilane coated portion of the channel has hydrophobic character while the uncoated portion of the channel remains hydrophilic, this treatment creates a wetting phenomenon where the aqueous stream has an affinity for the uncoated glass while the organic solution has an affinity for the alkylsilane coated portion of the channel. This greatly aids in separation since the outlet ports are coated to allow the selective passage of either aqueous or organic solvents. These separation systems are not practical for continuous synthesis reactions because under harsh conditions, such as high temperature, acidic or basic media promotes the hydrolysis of the silane groups, thus removing the coating over time. Loss of separation ability due to degradation makes this technique impossible for continuous flow applications.

Guideline structures are another interesting use of pillars to influence liquid-liquid flows. Pillars are fabricated along the center length of a channel to stabilize the immiscible liquid-liquid interfaces. The stabilization results in an overall increase in the separation efficiency of the device, where the immiscible fluids are directed toward their respective outlets selectively. Yamada[65] fabricated glass microfluidic devices containing guideline structures which maintain efficient phase contact for the hydrolysis of benzyl chloride to occur with a higher yield (13%, 1.3s residence time) in the microfluidic device than is afforded by batch techniques alone (>1%, 1.4s residence time).

Distillations are based upon the removal of a single compound from a mixture using the relative difference in boiling points. This principle has been applied to microfluidic devices for removal of components for subsequent analysis. Yang and Fu successfully used a microfluidic device to remove SO_2 from H_2O using distillation with an 94.6% efficiency, they subsequently

used their device to measure SO_2 concentrations in wine.[66] Although microfluidic distillation has the benefits of low sample volume, fast response time and high separation of components, it is limited to low boiling point liquids and is not a continuous method. The most promising type of microfluidic two component separation is capillary pressure continuous liquid-liquid separation.

Capillary separations of immiscible flows are based upon the capillary pressure generated by solvents through extremely thin tubes. The Young-Laplace equation (Equation 4), describes the capillary pressure required to push a fluid through a small diameter tube, where p_c is capillary pressure, γ is interfacial tension between the two fluids of interest, θ is the contact angle of the liquid with the capillary tube material and r is the radius of the capillary tube.

$$p_c = \frac{2\gamma \cos\theta}{r} \qquad (4)$$

The Young-Laplace equation allows for the prediction of the pressure necessary to selectively push fluids through the capillary opening which is termed the 'break through pressure'. Break through pressure (p_b) is the pressure above which the higher surface tension liquid (water) will begin to flow through the capillary channel, while below p_b the lower surface tension liquid (oil) will flow through the capillary channel. This type of separation has been mostly studied employing simple pure oil and water as proof of concept systems using both PDMS[67,68] and porous Teflon membranes[69] as capillary separators. The use of capillary separators is also aided by the wetting properties of the capillary material, which can be accomplished using hydrophobic material such as PTFE, producing contact angles of 108° with water and 41° with hexadecane[70] (Figure 10).

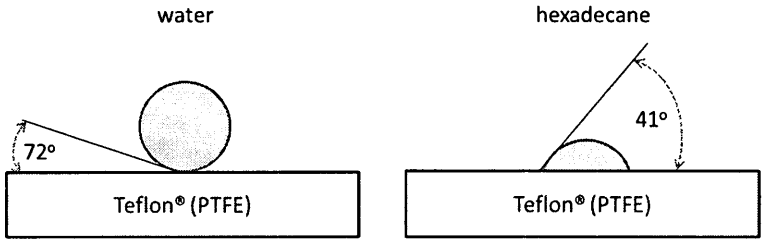

Figure 10: Depictions demonstrating the contact angle measurements of water and hexadecane droplets on untreated PTFE surfaces.

The contact angle of liquids with surfaces becomes a prominent factor on the microscale, where the contact surface area between the wetted surface and the liquid is very large while the bulk properties of the liquid are largely suppressed. Larger contact angles result in a higher p_b required to push the non-wetting liquid, such as H_2O and DMSO, through a capillary channel, when PTFE is employed. Solvents such as ethyl acetate, hexanes and hexadecane have low contact angles with PTFE due to Van der Walls interactions which result in much lower p_b. The lower breakthrough pressure allows the organic solvent with lower surface tension and lower wetting angle characteristics to selectively flow through small channels with hydrophobic surface properties, within certain pressure ranges.

1.7 Bi-Phasic Phase-Switching Extraction Strategies

The use of chemical extraction is a central practical aspect of chemistry and one of the most used techniques while performing a chemical transformation. Two phase extractions involve the use of acidic, basic or neutral aqueous media with an immiscible organic solvent reaction mixture (Figure 11). This can be combined with a quench step and an extraction step to remove spent inorganic reagents or by-products.

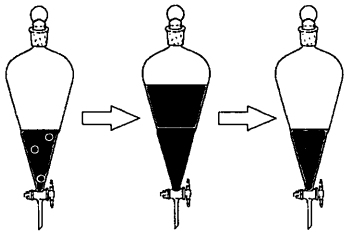

Figure 11: General schematic involving extraction of preferentially soluble species from a reaction mixture. A reaction mixture once maximum conversion is reached is often quenched with acidic or basic aqueous solution, resulting in the halt of the activity of the reagents, this usually also results in the removal of aqueous soluble by-products or reagents.

Reaction workups provide a major removal process for unwanted inorganic reaction components before undergoing chromatographic separation, where extraction of impurities through acidic or basic media can run as high as 99% depending upon *pKa* values of the components. Since efficient extraction is necessary to traditional applied chemistry, it is also important in continuous flow systems to obtain the desired product.

When performing biphasic extractions there must be a consideration of the partitioning behaviour of the compound of interest and by-products between organic and aqueous layers. The partitioning coefficient (*P*) (Equation 5) refers to the equilibrium mass partitioning of dissolved molecules between two immiscible phases in contact with one another.

$$\log P_{org/water} = \log\left(\frac{[solute]_{org}}{[solute]_{water}}\right) \qquad (5)$$

When subjecting an organic solution to aqueous partitioning conditions, appropriate pH, volume, and number of washes to obtain the product while minimizing by-products must be considered. For highly efficient phase-switching between neutral aqueous solvent and organic solution the minimum is $log\ P > 1$, based on a logarithmic scale. Although the use of non-ideal boronic acid derivatives with log P values >1.2 would be sufficient to obtain adequate recovery of the product

using experimental techniques. The *pKa* of the target molecule and by-products must be known, since the formation of cationic or anionic charges greatly increases solubility in aqueous solution (Figure 12) due to increased solvation by water.

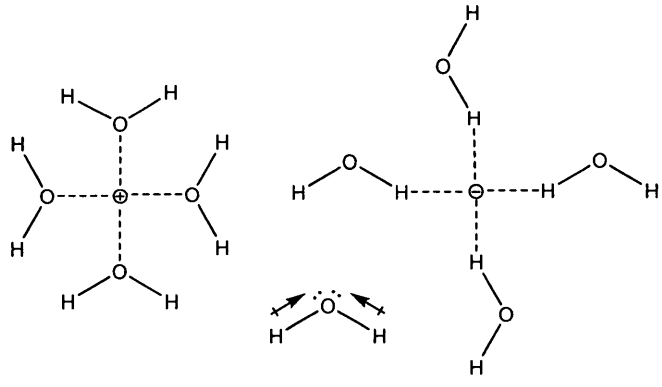

Figure 12: Solvent cages generated by the solvation of ions by water can vary in the number of water molecules depending upon the charge size. Solvation is a result of the strong dipole interaction of water with ionic species.

Acid-base extractions are the simplest form of reaction purification and rely on the generation of ionic species to phase-switch molecules between immiscible aqueous and organic phases (Figure 12). This method of crude purification is usually followed by use of chromatographic resolution using copious amounts of eluent solvent to remove neutral impurities. These extractions are largely based upon *pKa* (Equation 6), where ionic groups, either cationic or anionic, increase the solubility of aliphatic compounds through strong solvation with water.

$$pK_a = -\log \frac{[H^+][A^-]}{[AH]} \qquad (6)$$

If the molecule is ionisable, this results in the conjugate base or conjugate acid being more soluble in aqueous media. Greasy or aliphatic molecules partition solely through *log P*, and have very low solubility in polar solvents. With the development of fluidic technologies, there is a

growing interest to incorporate extraction and phase-switching strategies into continuous flow systems to streamline and automate synthesis.

Molecular tagging strategies (Figure 13) involve the use of covalently bonded functional groups that impart selective solubility or interactive properties with 'click' conditions. This separates the desired substrate from other materials, such as spent reagents, by-products and reaction solvent for purification purposes without using chromatography.

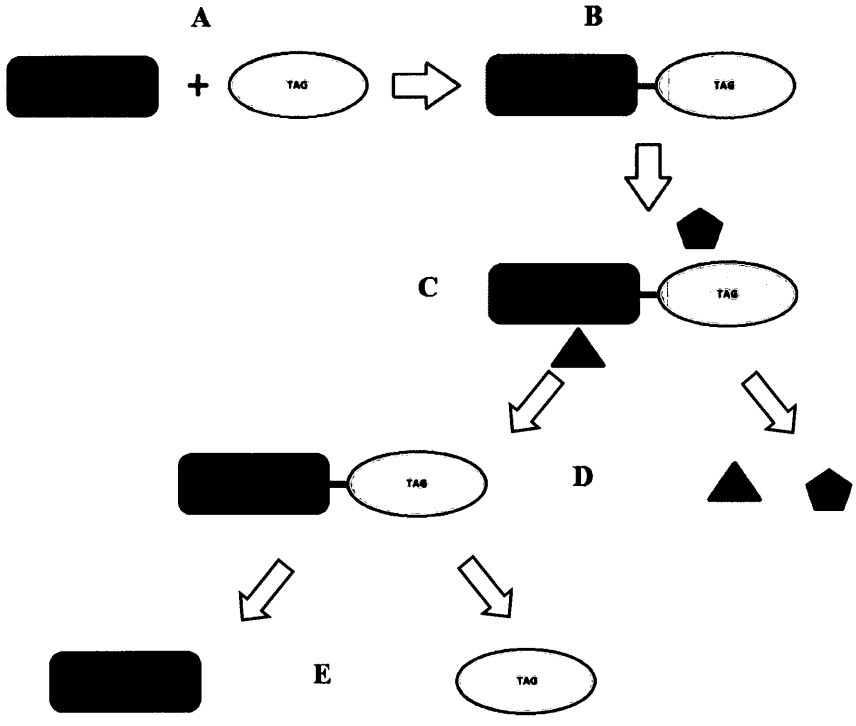

Figure 13: Depiction of a general tagging purification strategy. (A) The general 'tagging' strategy involves covalent bonding of the 'tag' molecule with a substrate molecule for purification after a subsequent chemical transformation. (B) The tagged substrate is then subjected to a chemical transformation to produce the tagged modified substrate (C). After the reaction is complete the 'tag' functionality is used to separate the tagged molecule from the reaction impurities (D), typically through solid support binding, chromatography or solubility. The final step is the removal of the 'tag' from the modified substrate using a clean cleaving method (E).

This methodology has been explored using covalently bound fluorous tags, which are fluorinated functional groups that are only soluble in fluorous solvents. Purification using this method have been used as monolithic chromatographic material,[71,72] fluorous tagged reagents for subsequent product purification,[73] carbohydrate purification,[74] fluorous tagged palladium catalyst complexes for catalyst recycling,[75] ionic copper chelators as 'catch and release' strategies,[76] click strategies with Ruthenium ligands,[77] redox switchable tags[78] and microgel polymer supports.[79] Fluorous tagging has proven to be the most efficient method to date, involving preferential dissolution of fluorous tagged molecules or complexes in fluorous solvents for selective extraction from reaction mixtures. Current fluorous tagging strategies are limited in scope, since fluorinated compounds are generally expensive, introduce inefficient atom usage, expensive disposal requirements and are considered hazardous materials. As a result, these techniques will not find mainstream acceptance in either academic or industrial laboratories due to their inherent limitations. The requirements of tagging strategies introduce two unproductive steps: attachment and subsequent removal to produce the final product. If these steps can be minimized or utilized effectively without adding synthetic steps they would provide a powerful tool.

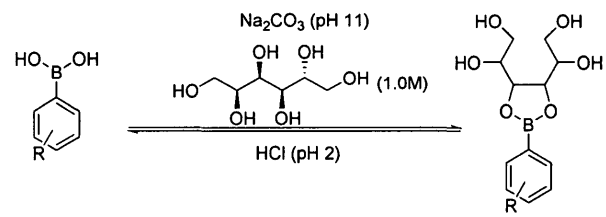

Figure 14: Phase-switching protocol for the reversible removal of p-tolylboronic acid from an organic solvent into an aqueous phase under base conditions, then hydrolyzed back to boronic acid using acid and dissolved into an organic solvent.

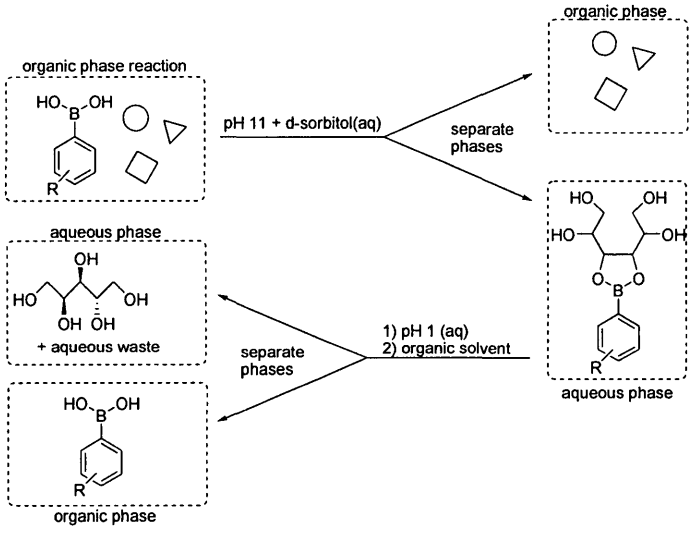

Figure 15: Schematic for the workup of reaction mixtures of boronic acids using water soluble boronate esters with liquid-liquid extractions to facilitate purification. Under Dennis Hall et al. conditions starting at top left, an organic reaction mixture containing the boronic acid labelled molecule and impurities is treated in a separatory funnel with an aqueous (pH 11-13) solution of 1.0M D-sorbitol and shaken for 5 minutes. The phases are separated and the organic phase is discarded, but the aqueous solution is then acidified to pH 1-3 and fresh organic solvent is added and then shaken. The resulting aqueous solution is discarded and the organic solution is dried to obtain the boronic acid labelled molecule.

Recently developments towards making more efficient and useful tagging strategies have been developed using boronic acids for phase-switching tags under homogeneous conditions (Figure 14) by Dennis Hall.[80] This method uses organic soluble aryl substrates containing boronic acid functionalities in conjunction with polyols under basic aqueous conditions to form water soluble boronic esters. These diffuse through the interface into aqueous solution, then combined with fresh organic solvent and are acidified to provide the hydrolyzed boronic acid, which are dissolved into the clean organic solvent (Figure 15). Arylboronic acids are suited towards phase-switching methodologies since they perform well under aqueous basic and acidic conditions and a variety of reaction conditions, display more efficient atom economies, are relatively non-toxic, and undergo 'click' conditions.

Hall demonstrated that arylboronic acids are stable to a variety of reaction conditions such as IBX oxidations, DIBAL-H reductions, esterifcation of alcohols, amidations, Wittig reactions, and Grignard additions.[81] This demonstrates that arylboronic acids are stable to harsh reaction conditions without the use of protecting groups. Arylboronic acid tagging strategies also show good atom economy as opposed to other tagging methods because the tag can be utilized in chemical transformations such as Suzuki cross-coupling,[82] Rhodium cross-coupling (C-N and C-C), chemoselective oxidations,[83] catalytic hydrogenations,[84] selective aerobic oxidative coupling,[85] transition-metal free cross-coupling[86] and protodeboronation to name a few.

The use of arylboronic acid moieties as phase-switching handles adds synthetic utility while reducing synthetic steps such as protection protocols for subsequent column chromatography. Purification of most boronic acids is difficult since they are highly polar, like carboxylic acids and adhere to polar chromatography material such as silica. The degree of lipophilicity of the boronic acid substituent influences chromatographic adhesion, where highly lipophilic substituents decrease retention on silica. Another method to decrease polarity is boronic acid protection using a 1,2 diols such catechol and pinacol esters to mask the polar hydroxyl groups as lipophilic esters.[87]

Lastly, boronic acid phase-switching handles are beneficial since extraction of the hydrophilic boronic ester is a 'click' reaction which can be combined with workup schemes. Since the phase switching protocol occurs using a polyol under aqueous basic conditions, this methodology can also act as an integrated workup scheme. Treatment with acidic aqueous media can also act as a second workup to retain impurities by solvating ionic species while pushing the lipophilic hydrolyzed boronic acid into the fresh organic phase. These phase-switching adducts can be considered triggered or 'click' conditions because initiation occurs only in the presence of

a suitable polyol with a 1,2 syn-diol motif. Therefore it is possible to develop unique workup and phase-switching conditions to suit specific reaction conditions.

The use of sugars for solubilizing boronic esters for the reversible extraction of boronic acids is based upon 1,2 syn-diol sugar interactions acids has been exploited as enzyme inhibitors,[88,89] saccharide sensors,[90,91] controlled feedback delivery for insulin,[92] and boronolectins for cell surface marker recognition.[93]

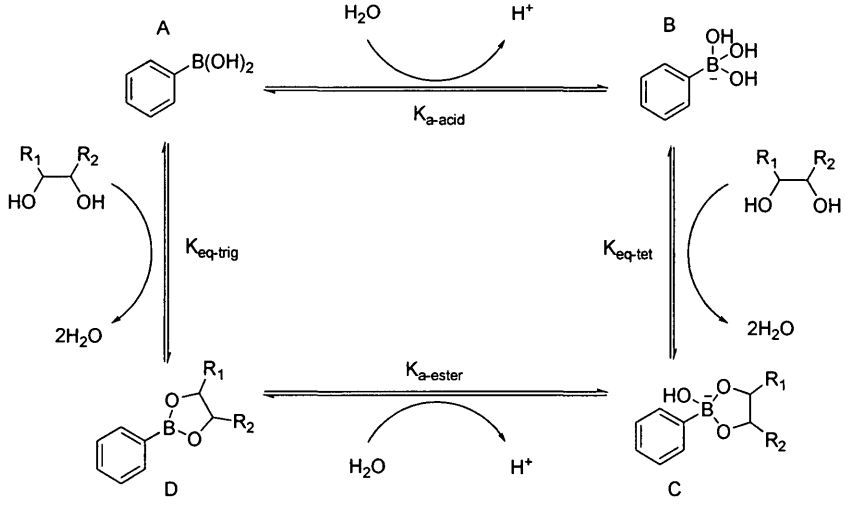

Figure 16: Competing boronic acid complexation pathways with 1,2 diols under neutral and basic conditions.

The reversible interaction of vicinal diol moieties such as sugars with boronic acids (Figure 16) was first studied by Lorand and Edwards[94] using a pH depression method to determine the mechanism of ester formation. It was determined that ester formation was more favourable in higher pH solutions where boronate ions (Figure 16B) exist in higher concentrations. This study showed that ester formation can go through two competing pathways ($K_{eq\text{-}tet}$ or $K_{eq\text{-}trig}$) (Figure 16) to obtain the same ester product but as pH increases the $K_{eq\text{-}tet}$ pathway becomes more prominent and results in faster ester formation. It was also shown that ester formation is faster under high pH conditions because of the release of ring strain (120° to 109°) through favourable tetrahedral

hydroxyboronate ion formation (Figure 16 B-C) due to increased Lewis acidity of the ester product.

Boronate ester formation from diols has been shown to be selective for syn 1,2 diols over other hydroxyl moieties. The selectivity of boronic acids for syn 1,2 diols over 1,2 trans diols and 1,3 diols arises because of the planer configuration of the neutral boronic ester product. While trans diols introduce more ring strain into 5-6 member esters than syn diols, although these are fast processes under high pH conditions, these processes are under thermodynamic control, which will tend to produce the most stable product in a complex mixture of polyols.

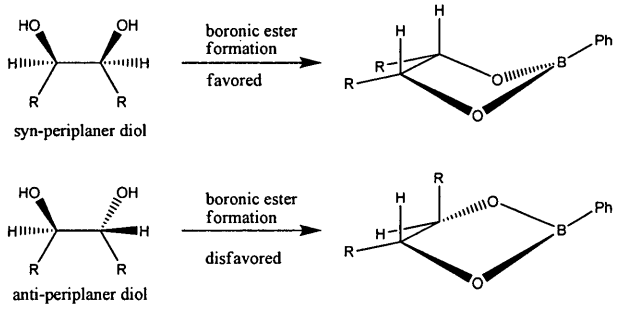

Figure 17: Depiction of syn-periplaner diols with both substituents on the same side of the molecule, while anti-periplaner groups have the substituents on opposing sides of the molecule complexiing with an arylboronic acid. Syn-diols complex quickly to form lower strain boronic esters (top), while trans-diols are much slower to complex with boronic acids to produce the ester because of additional ring strain.

The polyol structure is a major concern for the complete conversion of arylboronic acid to the corresponding ester (Figure 18). It was determined by Hall, that D-sorbitol was the most efficient polyol for the complete conversion to the corresponding ester of a variety of simple non-orthosubstituted boronic acid derivatives (Figure 18), by comparing recovery yields of the boronic acid. A comparison of D-sorbitol, glucose, mannitol, polyvinyl alcohol, and fructose elucidated that D-sorbitol gave the best recovery yields due to the C3, C4, C5 syn triol motif (Figure 19) and linear flexibility which other substrates lack. D-sorbitol is a more efficient

reagent since the linear form has more degrees of freedom as opposed to the restricted ring form of D-glucose.

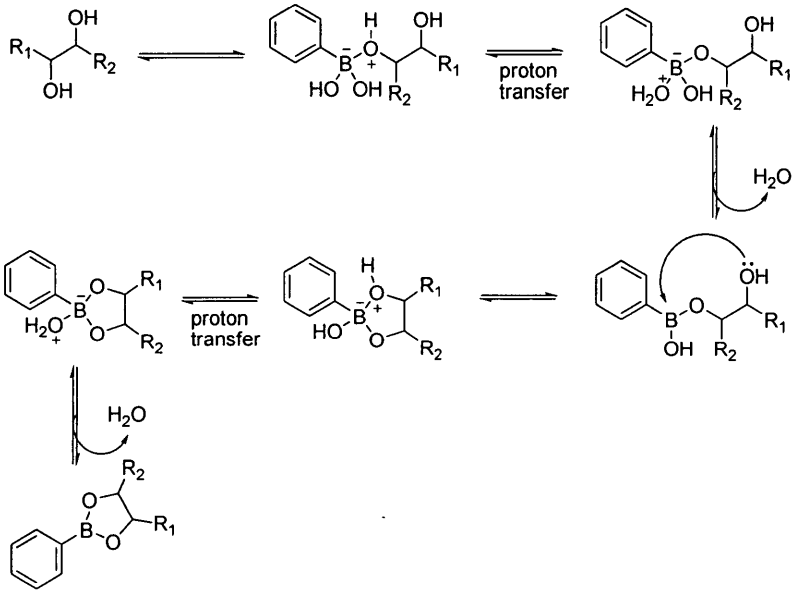

Figure 18: Formation of neutral boronate esters by dehydration of unhindered arylboronic acids and 1,2 diols.

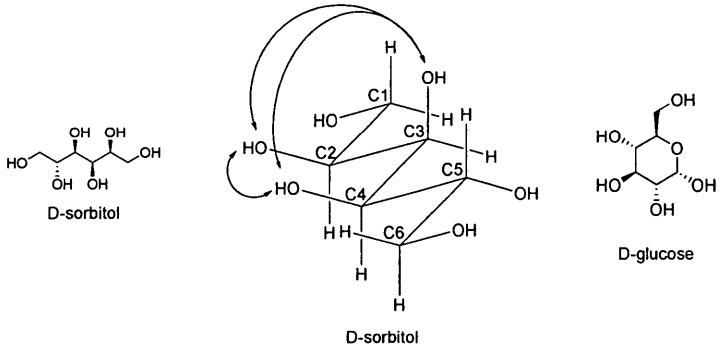

Figure 19: Structures of D-sorbitol and glucose. With a 3-D diagram of the C2, C3, and C4 hydroxyl steric interactions.

Boronic ester formation is further aided by the steric interactions of D-sorbitol between the hydroxyl groups which produces a bow shape to the molecule, the bow effect reduces steric hindrance of the remaining trans-hydroxyls and carbons by pushing them back and away from the C2, C3, and C4 hydroxyl groups allowing a faster and less hindered interaction with the incoming boronic acid.

1.8 Incorporation of Boronic Acid ``Tagging`` Molecules for Selective Phase-switching into Microfluidics

The incorporation of batch vessel chemistry into flow devices has been successful in delivering cleaner reactions, reduced waste, shorter optimization times, continuous separation of organic/aqueous phases and easy scale out. The use of one step reactions in microflow environments severely limits the usefulness of flow reactions, where reaction quenching and workup are considered secondary batch processes only to be completed after collection of the reaction mixture. If microflow reactions are collected into batch vials, without inline quenching or workup, most of the benefits garnered by microreactors are lost.

By using microflow devices to facilitate boronic acid phase-switching, aliquots of reaction mixtures can be diverted from reaction flow streams as either slugs or continuously to undergo dilution and crude purification using two-phase phase-switching and continuous capillary separation. This crude material can then be injected into mass spectrometer systems for analysis (Figure 20).

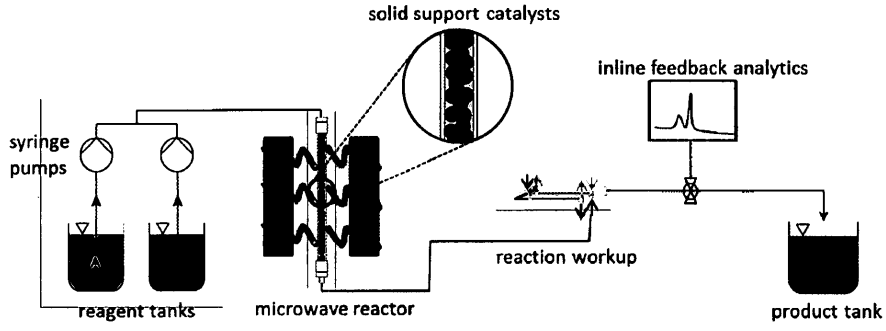

Figure 20: Incorporation of microfluidic reaction workup module between a microwave reactor and collection tank to flow crudely purified product to analytics for automated feedback optimization and GMP documentation of flow.

These types of purification systems for real time analysis are sorely needed, since reaction mixtures cannot be directly injected into MS systems because harsh reagents, salts or water can damage or illicit poor MS signal response. Hence microfluidic devices allow faster analyte response for continuous flow monitoring.

1.9 Plan of Study

The aim of this investigation is to utilize microfluidics to quickly prepare two-phase reactions and separate phases inline under laminar flow conditions. This project involved the design and fabrication of a novel microfluidic reactor, then incorporating a boronic acid phase switching methodology introduced by Hall et al to produce a fast inline purification method for continuous microreactors. This protocol uses pH reversible hydrophobic boronic acid functionalization with syn-diol containing polyols to create hydrophilic boronic esters. The boronic acid phase switching methodology has been shown to be effective for the crude purification of synthetic intermediates in the synthesis of ezetimibie and still achieve good yields without chromatography.[95] The use of laminar flow in this context will allow us to incorporate the batch phase switch chemistry into a flowed regime. By combining these technologies and techniques we hope to develop a unique system for the real time crude purification of reaction

products in flow reactors to reduce manufacturing costs and increase efficiency to challenge batch reactors in large scale chemical production, which relies heavily on chromatographic separation.

To demonstrate the utility and function of the proposed fluidic system, organic solutions of arylboronic acids with basic aqueous solutions of polyols will be flowed together, forming boronate esters at the interface of the stratified flows. The newly formed boronate ester is much more soluble in aqueous media and will diffuse into the aqueous stream, while the organic waste stream is removed using capillary action. The aqueous stream which contains the aqueous soluble boronate ester is then merged with an acidic aqueous stream and organic solvent which hydrolyzes the boronic ester and diffuses into the fresh organic stream. The binary flow is spilt again using capillary action to obtain the organic fraction containing the dissolved arylboronic acid and separated aqueous fraction, for collection and analysis.

Chapter 2

2.0 Results and Discussion

2.1 Development of a Two Unit Operation Fluidic Device

A number of issues concerning the application of boronic acid phase-switching to microfluidic conditions need to be addressed for optimization of two phase separations while retaining chemical utility. Two primary areas of concern involve microfluidic network design and chemical behaviour inside of micron sized channels. First the fluidic design must be able to operate using moderate flow rates to produce significant amounts of material with an appropriate residence time and operate at lower backpressures to facilitate efficiency phase separation using capillary action. The optimal conditions need to be determined to maximize overall mass yields per unit time, retain solubility of intermediates and products, minimize side reactions and eliminate undesirable species, such as gases or precipitates. System solubility and backpressure are the most important parameters because any formation of solids in the microchannel can lead to blockages, which adversely increases system backpressure and, therefore the system needs to maintain liquid homogeneity.

2.2 Theoretical Reactor Design Calculations

To properly design any microfluidic device some estimation is required regarding the translation of batch reactor unit operations into a microfluidic reactor. To determine theoretical optimal chemical conditions in a microreactor, some theoretical values need to be determined such as, Reynolds number, backpressure, diffusion coefficients, and diffusion time required for reaction completion. P-tolyl boronic acid (pBA) was a substrate for modeling and testing of device efficacy and phase-switching yields since it is a well-known substrate, commercially available and has a favourable logP. To determine optimal residence time for complete reaction

and extraction appropriate flow rate ranges need to be found using the estimated diffusion coefficient of pBA. The diffusion coefficient of pBA was modeled using an approximation of Stokes Radii or hydrodynamic radius since this data is not available from the literature. Stokes Radii of pBA was estimated to be 6 Angstroms, similar to other small molecules such as Raffinose, which is an intentional overestimation of hydrodynamic radius. Using the estimated hydrodynamic radii, we calculated a diffusion coefficient D of 2.55E-9m^2s^{-1} (calculation see appendix).

Table 1. Experimentally obtained log P values for p-tolylboronic acid, using standard shake flask method; followed by vacuum drying of organic layer to determine mass recovery.

Initial Mass (mg)	Volume Ethyl Acetate (mL)	Volume Distilled H_2O (mL)	Final Mass in Ethyl Acetate (mg)	Log P
97.8	10.0	10.0	94.4	1.44
85.7	10.0	10.0	80.3	1.17
71.3	10.0	10.0	67.1	1.20

Average log P calculation with standard deviation = 1.27 ± 0.15 (for calculations see appendix)

Table 2. Experimentally obtained log P values for 2-napthylboronic acid, using standard shake flask method, followed by vacuum drying of organic layer to determine mass recovery.

Initial Mass (mg)	Volume Ethyl Acetate (mL)	Volume Distilled H_2O (mL)	Final Mass in Ethyl Acetate (mg)	Log P
699.9	110	375	527.7	1.02
597.3	110	210	537.6	1.23
307.0	75.0	140	283.8	1.35

Average log P calculation with standard deviation = 1.20 ± 0.17 (for calculations see appendix)

With the estimated *D*, we proceeded to model the fluidic device dimensions by calculating Reynolds number (Eq. 3), maximum residence time required for complete diffusion (Eq. 4), along with backpressure using the Poiseuille equation (Eq. 1) to achieve a rough estimate for successful capillary separation of binary phases. Although much iteration of channel lengths and cross-sections were experimentally explored, the optimized channel dimensions were determined to be 0.51mm height, 0.51mm width and a fixed length of 30.5cm with a maximum residence time of 25.2 seconds (calculation see appendix) for complete diffusion of pBA, while maintaining a low backpressure for capillary phase separation. The calculation of diffusion time was used as the baseline residence time for our flow studies, assuming diffusion is the limiting

step, since the calculated Reynolds number was 3.2 (see appendix for calculation), indicating it operated completely under laminar flow with diffusion as the main method of mixing.

2.3 Evolution of Tandem Extraction Two-phase Microfluidic Devices

The initial flow device (1st generation) was designed around a compression chuck with the channel substrates consisting of engraved PTFE and glass using Y-junctions for contacting two immiscible phases, followed by a straight reaction channel to allow conversion and extraction of the target arylboronic acid, and concluded with a Y-junction in the hopes of splitting the concurrent flows into separate pure streams. This device was quickly scrapped due to technical and practical difficulties and replaced with a steel chuck-gasket design. The 2nd generation device provided leak proof flow and flexibility over the previous device but insufficient reactor space produced low residence times and lacked efficient binary phase separation. A 3rd generation device with an improved design based upon the previous device contained flexible port configurations, longer channel lengths and space to incorporate capillary phase separation channels. By expanding the flow network to include a second inline transformation, the injection of additional reagents and solvent through a T-junction port the final 3rd generation device proved to be a successful design. To develop these devices we used laser ablation which is a simple and inexpensive method to fabricate microchannels in PTFE.

2.4 General Method to Fabricate PTFE Reactor Microchannels Using Laser Ablation

The fabrication of microstructures in PTFE was achieved using laser engraving facilitated with a Versalaser ™ 2.30 with a 30W laser module and simple computer software (Corel Draw 9) to generate and apply two dimensional designs. The PTFE sheets obtained from CS Hyde of known thickness (0.01"-0.03"+/- 0.001") were trimmed to the approximate overall size and

placed onto the laser cutting surface and reversibly secured using adhesive tape fix the PTFE sheet to prevent shifting and heat warping. Once the PTFE sheet is secured, the flow channels are made by loading a pre-made Corel Draw 9 design (.cdr) file into the Versalaser interface and selecting an appropriate laser settings (power and laser motion speed) to adjust the cutting depth and engraving width. All cutting and etching of channels involves the exclusive use of the vector laser mode, which experimentally is the best method for reliable fabrication of PTFE channels (see appendix). The Corel Draw 9 channel files are designed to fabricate channels as close to the desired widths and depths as possible through comparison of design cut widths and depths to measurements obtained with the final product gasket (see appendix for various cutting techniques and corresponding image and measurements).

The two-phase channels are created using rectangular vector lines with round 1mm diameter cut fluid connection ports. The rectangular cut shapes for the long channels is needed to make desired widths, because single line cuts do not produce the desired channel widths. The circular 1mm ports aid in the alignment of the stainless steel chuck fluid ports with the PTFE channels which minimizes distortion of the PTFE gasket from improper alignment or bunching of the gasket when the pressure screws are tightened. The most accurate channel widths are engraved using high laser power (30W vector setting), with only one laser pass. By using the fewest number of laser passes to remove channel material results in increased channel width accuracy, while increased laser passes causes a corresponding increase in the width of the channel, dependent upon laser power (see appendix). The channels do have considerable surface roughness due to a combination of deposited ablated PTFE particles and periodic waves in the side wall from the motion stepper motors which drive the laser axes. Typically channels are cut to approximately 0.5mm width with a PTFE film of 0.51mm thickness to achieve high surface

area contact of two-phase flows without generating high backpressure. These cutting methods generate a relatively clean cut profile (see appendix) where the removal of a thin strip of PTFE material from between the cutting lines forms the side walls of the channel. Once the two-phase flow channels are completed, capillary channels are engraved into the PTFE surface using lower power settings (vector plastic microsurface non-metallic +0% power) to produce shallow channels with a parabolic cross-section 0.27mm width and 0.27mm depth (appendix), without completely cutting through the PTFE film. The mentioned etch depth and width has resulted in the best separations of water, hexane and water, ethyl acetate binary phase mixtures. Smaller capillary channels result in insufficient phase separation from high break through pressure, while larger channels allow the passage of water at low flow rates due to low breakthrough pressure resulting in poor phase separation.

Once the binary reactor channels and capillary channels are ablated the final task involves cutting the gasket outline from the bulk film. This requires a high laser settings similar to those used to form the two phase reactor channels (32.0cm length and 3.8cm in width) of the entire gasket from the bulk PTFE sheet. Once the gasket has been carefully removed from the cutting stage the remaining ablated particulate matter is removed by sonication in a bath of distilled water for 5 minutes, followed by sonication in methanol for 5 minutes. After cleaning is complete the PTFE gasket can be placed inside the chuck for assembly (see appendix).

2.5 First Generation Microfluidic Device Single Unit Operation Device

Our initial microfluidic device was composed of a block PTFE bottom (Figure 20A) and a glass top (Figure 20B) two layer design, where the two bulk materials were laser engraved with microstructures to form channels once assembled. The microchannels were formed by engraving

a ¼" PTFE block and a ¼" slide of borosilicate glass using a computer controlled laser engraving machine (Versalaser 2.30), with metal capillary fluid connections embedded into the PTFE material using heat welding. The etched channels (Figure 21C) were then aligned using an optical microscope and clamped together under pressure (Figure 22D) to form the microchannels (Figure21 C). This design was intended to operate through selective wetting of the channel surfaces, where aqueous solutions would selectively wet the glass surface while the organic solution would preferentially wet PTFE surfaces, resulting in binary concurrent laminar flow and phase separation using flow splitting.

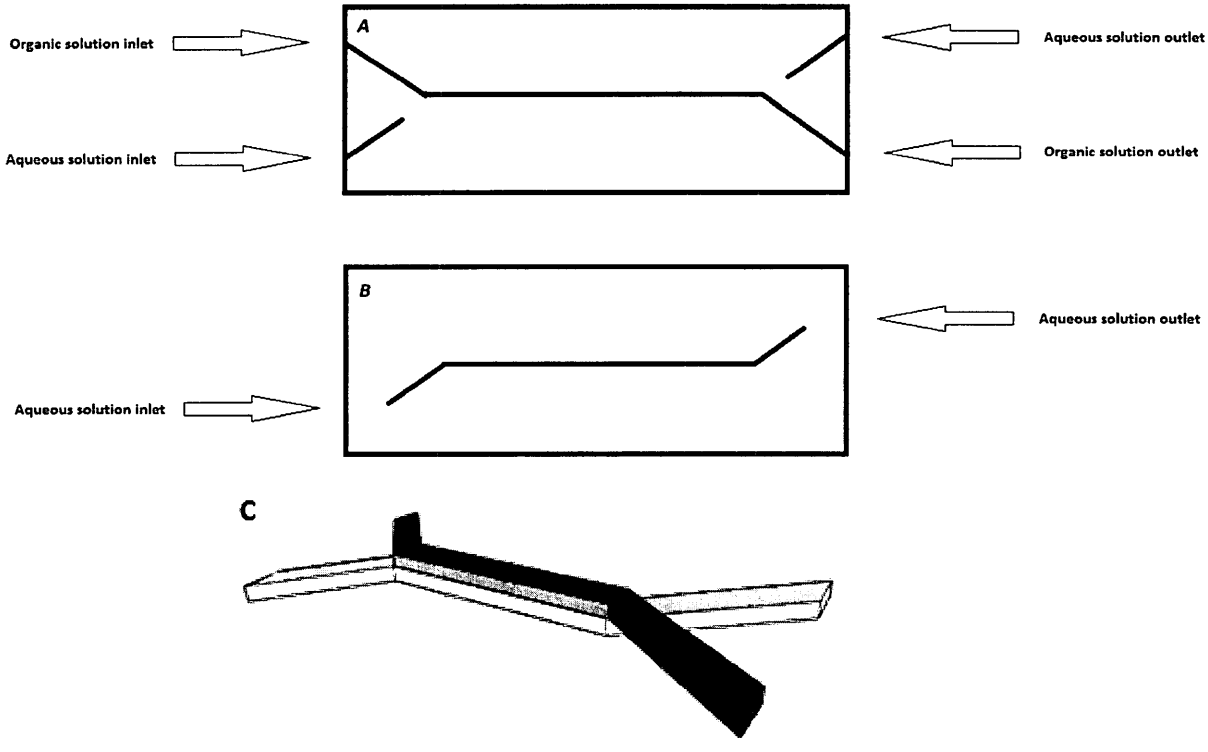

Figure 21: Depiction of 1st generation microfluidic device design. *A*) is the top surface of a PTFE block, black lines indicate laser engraved microchannels at high power (30W vector). B) depicts the bottom glass substrate, with a mirrored laser etched channel. C) depicts the overlap of the microchannels once assembled in the pressure plates (Figure 19C).

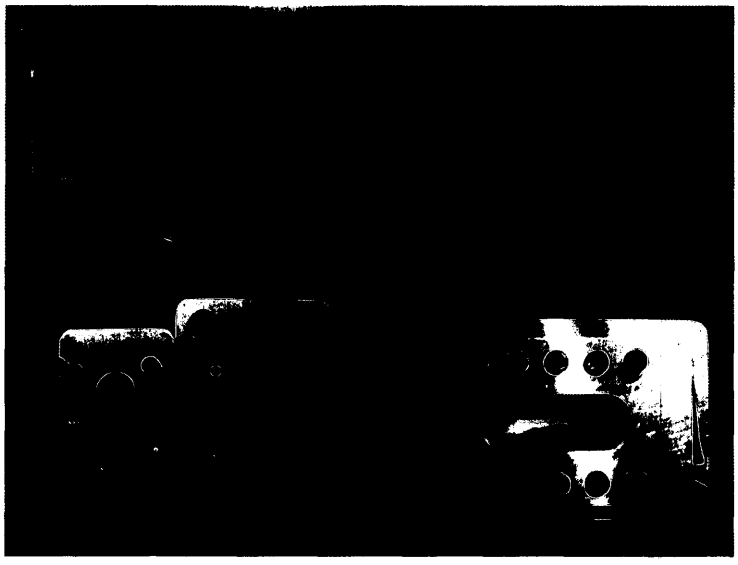

Figure 22: Images of 1st generation fluidic device components. A) laser engraved glass microchannel. B) Laser etched PTFE microchannel, and heat embedded steel capillary fluid connections. C) stainless steel compression plates, used to pressure seal PTFE and glass blocks together to form the microchannel. D) assembled microfluidic device with blue nitrile gloves acting as a cushion to prevent glass plate breakage once pressure is applied.

PTFE and glass were chosen as substrate materials because of high corrosion resistance, commercial availability and ease of channel fabrication using laser ablation. This design was tested under two-phase flow conditions, with ethyl acetate and water to simulate reaction conditions using a variety of flow rates but the design suffered uncontrollable leakage and lack of adequate phase separation ability. The leakage could not be stopped because high pressure exerted by the assembly chuck (Figure 22D) resulted in glass substrate breakage. This prompted us to adopt a more robust design without using brittle materials, while addressing the need to incorporate the second reaction step; therefore a more flexible and robust design was required.

2.6 Second Generation Single Unit Operation Device

The 2nd generation device design was a complete departure from the previous device, using a single layer of PTFE to form microchannels. The channels are efficiently formed using laser ablation (Versalaser 2.30) to engrave our microstructures into a thin PTFE film (CS Hyde).

This design needed to address problems encountered with the 1st generation device such as robustness, high internal pressure, easy microstructure fabrication, chemical resistance, operate at high flow rates while retaining long residence times and phase separation of immiscible liquids continuously. The choice to adopt a sandwiching stainless steel chuck design provided some benefits since it can incorporate standard high pressure HPLC fluid connectors and use high pressure to seal the microchannels by deforming the malleable PTFE film, which minimizes port leakage and channel leakage at high backpressures.

2.7 Construction of 2nd Generation Stainless Steel Chucks

The fluidic device consists of paired CNC machined 316 stainless steel chucks (Figure 23) and a single PTFE (Figure 25) gasket that forms the microchannel (Figure 24) inside of the assembly (Figure 26). The 316 stainless steel chuck supports 1/4"-28 threaded fluid connection ports to accommodate common HPLC fluid components and pressure screws to allow easy sealing of the PTFE gasket between the plates. The stainless steel chuck is capable of accommodating different PTFE gasket designs with a variety of channel dimensions and pathways. The individual machined plates have mirrored overlapping ports with a separation distance of 89mm and a diameter of 1mm. Once the plates are assembled the ports overlap to form T-junctions (Figure 24) at both inlets and outlets with an additional single port perpendicular to the outlet ports and offset by 10mm (Figure 23A, top left). The two overlapping inlet ports allow the generation of binary phase contact, while the outlet T-junction or incorporated capillary comb (using the offset port) are used to coalesce and separate phases for analysis or collection.

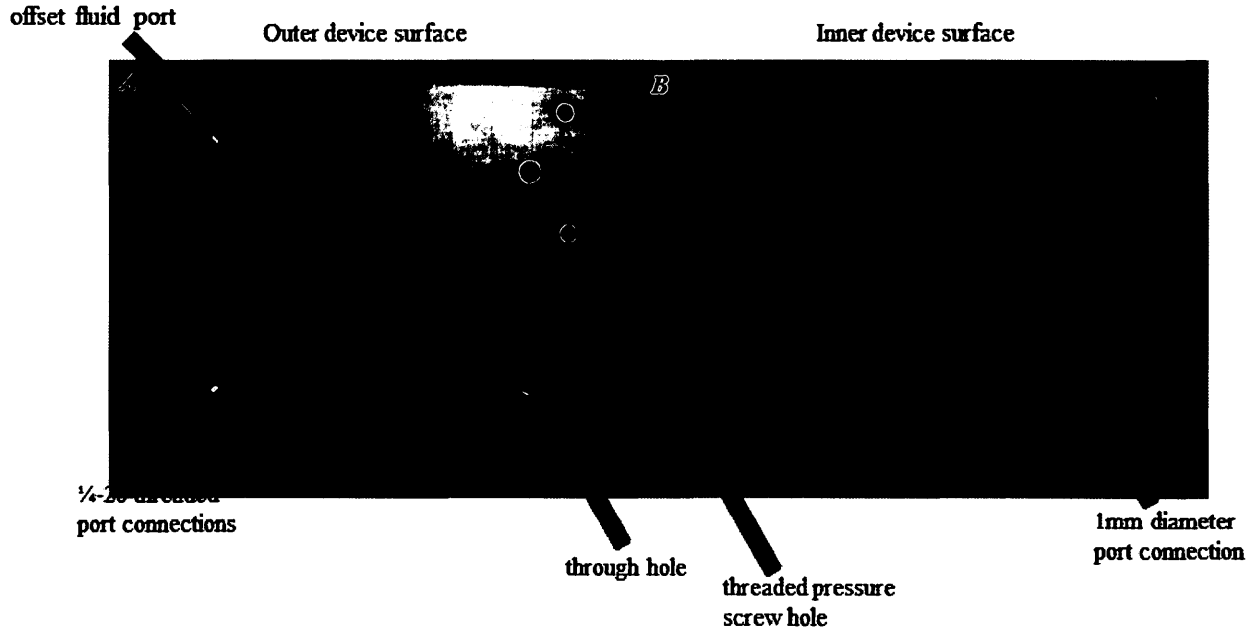

Figure 23: Photos of 2nd generation flow device chucks. *A*) outer surfaces of the two parallel 316 stainless steel plates, that have ¼-28 threaded ports to accept UpChurch PEEK fluid connection nuts for 1/16 outer diameter tubing. The bottom left plate has 6 smooth through holes around the plate edges, which are mirrored upon the top left plate with 10-32 threaded holes to accept screws to clamp the plates together with a PTFE gasket between. *B*) photos of the inner surfaces of the same two chucks which contact the PTFE film, which have 1mm diameter fluid holes to connect the external ¼-28 threaded ports to the fluid channels cut into the PTFE film.

2.8 2nd Generation Device Assembly

PTFE gasket microstructures were fabricated using the laser engraver to cut thin film PTFE material to produce a gasket-like sheets (Figure 25) containing microstructures of known height and width (see appendix) where excised material (negative space) forms the channels once the device is assembled (Figure 26). The inlet T-junction initiates the reaction by combining the immiscible phases causing the formation and extraction of the hydrophilic boronic ester from a combination of p-tolyl boronic acid in an organic solution and d-sorbitol under basic conditions at the fluid interface, while a T-junction at the outlet provides two flow channels to separate phases using differential backpressure generated by flow regulators.

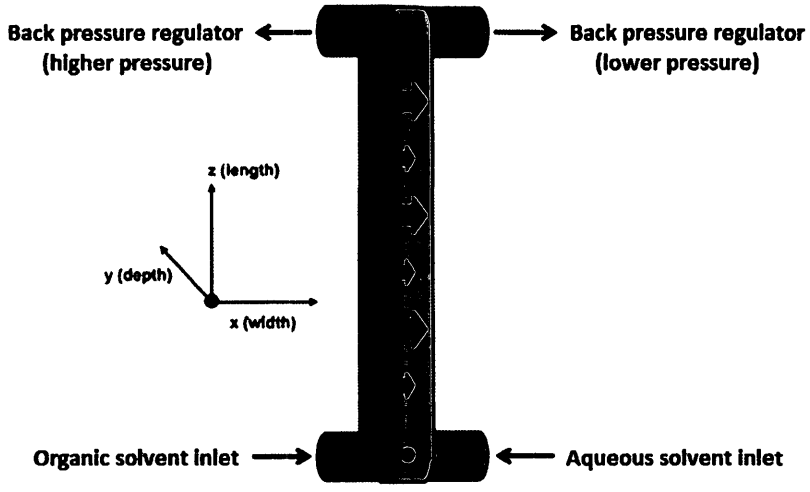

Figure 24: Depiction of the flow channel design of the assembled 2nd generation fluidic device. The bottom two overlapping inlets allow simultaneous infusion of solutions, the top two overlapping ports were to allow capillary separation of the two phases.[96]

The use of flow regulators (UpChurch Scientific Flow Regulator, P-446) to generate differential backpressure at the two flow outlets (Figure 24 top) aided significantly in the separation of binary phases consisting of pure solvents and the phase-switching reactions, where manual adjustments of the regulators resulted in much better separation efficiency.

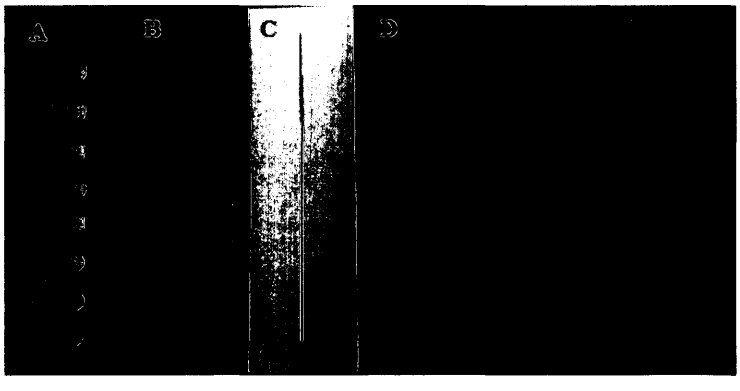

Figure 25: Photos of various PTFE films used as channel creating gaskets for inclusion in the 2nd generation stainless steel chuck. All PTFE sheets were obtained from CSHyde. A) 0.27 mm thickness, 0.59mm width, 30cm length serpentine channel. B) 0.27mm thickness, 0.22mm width, 9cm length. C) 0.80mm thickness, 0.53mm width, 9cm length. D) 0.45mm thickness, 2.23mm width, 9cm length. E) 0.27mm thickness, 3.76mm width, 9cm length. F) 0.27mm thickness, 8.18mm width, 9cm length.

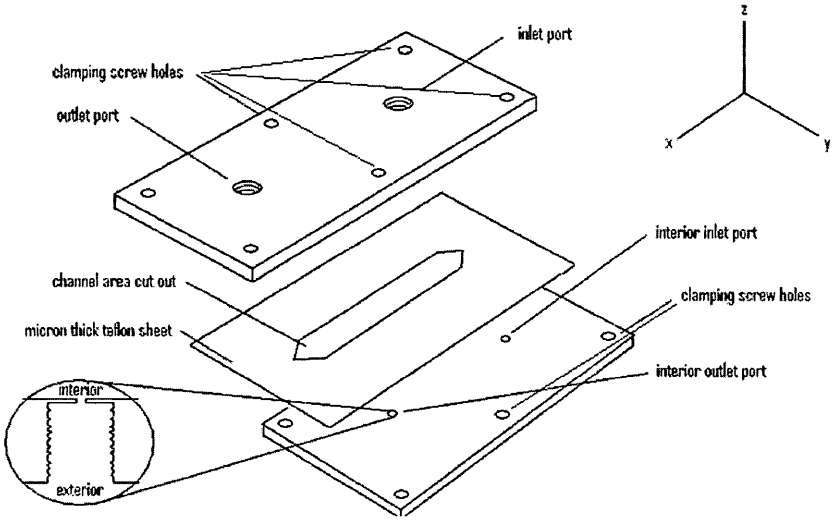

Figure 26. Exploded schematic of assembled 2nd generation microfluidic 316 stainless steel chip. Incorporates a channel length of 89.9mm and variable channel width and depth by varying laser cutting dimensions and Teflon sheet thickness respectively. Screws are used to pressure seal the device and ¼-28 PEEK fluid connections to 1/16 diameter PEEK tubing the using machined threaded ports.

2.9 2nd Generation Device Testing

Before reaction testing and optimization of the phase-switching reactions the 2nd generation fluidic device (Figure 26) binary phase separation was studied using pure liquids of ethyl acetate and distilled water (Table 3) to simulate similar conditions to the phase-switching parameters used by Hall et al.

Table 3: Separation Experiments of Ethyl acetate and Water in 2nd Generation Fluidic Device.

Entry	Total Flow Rate (μL/min)[a]	Outlet 1 Collection[b] (EtOAc:H_2O)	Outlet 2 Collection[b] (EtOAc:H_2O)	Calculated Back pressure (Pa)
1	10	50:50	0	1.0
2	20	50:50	0	2.0
3	50	50:50	0	5.1
4	150	50:50	60:40	15
5[c]	375	99:1	20:80	38
6[d]	375	99:1	50:50	38
7	380	71:28	35:65	39
8	400	55:45	50:50	41

The flow conditions involved a straight microchannel of 4mm width, 0.38mm height and 90mm length, with outlet tubing of 0.25, 0.5mm and a length of 78 and 322mm respectively. Both outlets had Upchurch Back Pressure Regulators (P-446) to make pressure adjustments for optimal separation conditions. a) total flow rate is the sum of the combined flow rates of the individual phases (EtOAc and H_2O) where all flow rates are 1:1 flow ratio. b) values represent the ratio of phases collected from the respective collection flasks, while zero represents no collected solvent was visually observed. c) These conditions were tests to determine separation efficiency based on flow orientation, with the axis of flow parallel to gravity, d) flow axis perpendicular to gravity.

The optimization of separation ability in the 2nd generation device was performed with fixed channel geometries (Table 3), while other channel designs were tested the results were similar in comparison. This demonstrates that a certain threshold of pressure is needed (Table 3, Entry 3) versus (Table 3, Entry 4) before solvent flow could occur through both outlet ports, but more importantly there is a transition to better phase separation (Table 3, Entries 5-7), while separation ability is lost once higher flow rates are reached (Table 3, Entry 8). This behaviour can be attributed to breakthrough pressure of the outlets which is low, since both outlets are 1mm in size. Calculations estimate that the operational window (water breakthrough pressure into the organic outlet) is approximately of 35-39 Pascals (calculation in appendix). The optimization of

the phase-switching reactions using optimal separation flow rates was difficult since residence time is low leading to a narrow range of high flow rates (Table 3, Entries 5-7). Then to study the correlation of channel dimensions to substrate recovery a range of microchannel designs (Figure 25) where fabricated (Table 4) using basic boronic ester extraction using the optimized flow separation conditions.

Using the optimized flow conditions from (Table 3) we tested hydrophilic boronic ester formation and extraction in flow using Halls methodology to determine the efficiency of recovery for the first step of the reaction using p-tolyl boronic acid in ethyl acetate (Table 4, Entry 1). The attempted optimization of reaction flow conditions (Table 4) demonstrates the difficulty of conducting two-phase flow reactions. Initially, we assumed binary flow behaviour was simple, with the placement of the inlets governing the arrangement of the fluids within the channel with high surface area contact but our experiments proved otherwise. The entries (Table 4, Entries 2,5) show that channel aspect ratio has large impact on recovery of the boronic acid, shown by the increase of recovery from 2-21% by decreasing the channel aspect ratio while maintaining the cross-section area of the channel, with a difference of residence time of 9 seconds. This could have resulted from rearrangement of the flow profile, where interfacial tension of contacted immiscible liquids is higher than individual solvent-air interfacial tension causing a rearrangement to occur resulting in lower surface tension due to lower surface area contact. The rearrangement minimizes interfacial contact area which lowers surface tension resulting in lower recovery under similar residence times and channel cross-section area from lower mass transfer rates. This prompted a study of lower aspect ratio (approx. 1) designs (Table 4, Entries 8-15), resulting in much higher recoveries, with drastically lower residence times of 5 seconds, with maximum recovery of 65% (Table 4, Entry 15). These results suggest future design

considerations must include shrinking the channel cross-section area but maintaining an approximate square shaped channel.

Table 4. Correlation table of residence time, aspect ratio and % recovery of p-tolylboronic acid using the Hall Protocol in flow.

Entry	Aspect Ratio (w/h)	Width (mm)	Height (mm)	Residence Time (s)[b]	Total Flow Rate (μL/min)	Recovery (%)[a]
1	-	-	-	-	-	92
2	210	16	0.076	46	140	2
3	31	8	0.254	110	100	12
4	31	8	0.254	78	140	14
5	15	4	0.254	54	100	21
6	2.6	1	0.381	22	90	-
7	2.6	1	0.381	17	120	27
8	1.3	0.5	0.381	7.3	140	45
9	1.3	0.5	0.381	6.4	160	36
10	1.3	0.5	0.381	5.7	180	29
11	1	0.4	0.4	6.5	120	54
12	0.85	0.2	0.254	2.5	120	35
13	0.85	0.2	0.254	3.0	100	53
14	0.85	0.2	0.254	3.7	80	62
15	0.85	0.2	0.254	5	60	65

(a) Recovery was determined using ^{1}H-NMR with anisole as an internal standard. (b) All residence times are calculated based on channel dimensions (see appendix). All boronate ester formation in the above table were performed using Table 1 entry 1 conditions. Reynolds number was calculated between $12 > Re > 3.2$ for the above channels, all conditions were therefore laminar ($Re < 2300$). Diffusion coefficient of p-tolylboronic was calculated to be $2.553 \times 10^{-9} m^2 s^{-1}$ using Stokes method (see appendix).

Subsequent experiments attempted to stabilize laminar flow to produce better phase separations using additional PTFE film layers, and multiple layer PTFE designs. These attempts to produce better phase separation using additional PTFE layers was hoped to provide selective wetting surfaces, where water wets stainless steel, while the organic layer preferentially wets the additional PTFE layer. Experimentally these added layers did not produce any beneficial binary phase separation effects under our flow conditions. Another attempted method of stabilization included the incorporation of guideline structures into the PTFE layer using various lasing techniques, such as staggered laser etches at different power settings to create guideline structures

and built up edges near the outlets to promote cleaner separations. These attempts did not provide any additional separation efficiency, although these designs produced fine micro-emulsions, which may have some value for other applications. With the 2nd generation device lacking an inadequate pressure operating window, low residence time and a second unit operation, a new device based upon 2nd generation network was built to address these problems.

2.10 3rd Generation Tandem Extraction Microflow Device

Development of the recent 3rd generation device was based on the need for longer residence times, higher channel backpressure and incorporation of a second unit operation. The overall channel length was increased to 330.2mm to include two straight reactor channels, 301.6mm and 279.4mm in length, which increases the operating window by lengthening residence time at higher flow rates, while producing higher relative backpressure. The inlet T-junctions (Figure 27) allow infusion of material through standard PEEK nut and ferrule connectors, while the outlets are capped with micro-capillary structures (Figure 27B) to selectively remove organic solvent (red) from the aqueous stream (blue), and the second tandem

channel mirrors this structure to carry out two reaction-extraction processes.

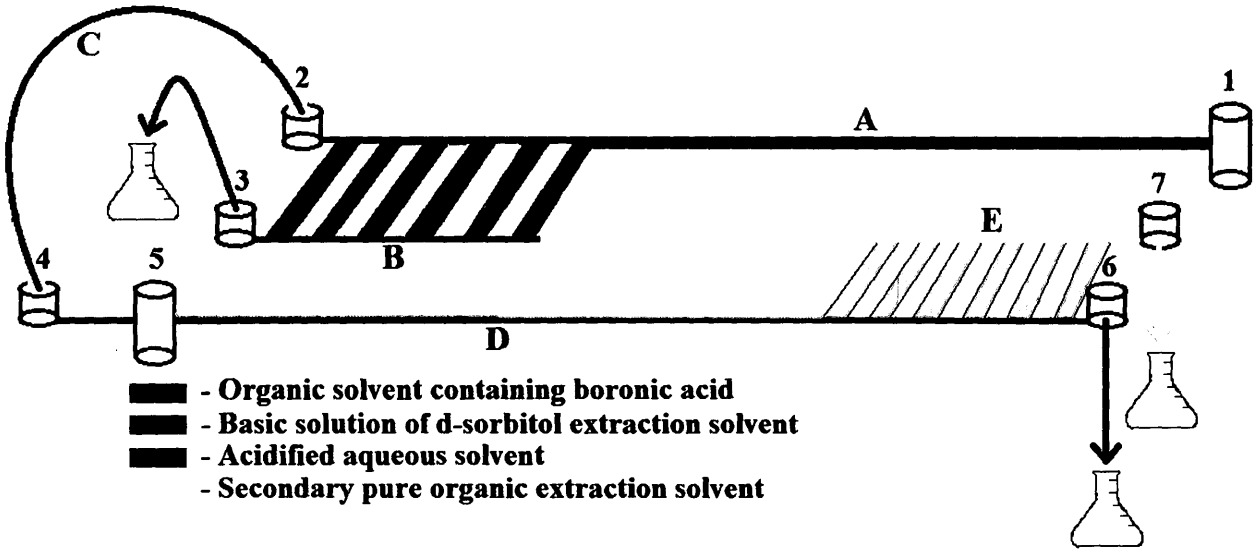

Figure 27: A simplified flow channel representation of our 3rd generation tandem extraction device. An organic reaction mixture containing the organic solvent soluble boronic acid product and a aqueous basic solution of d-sorbitol are injected (port 1). Simultaneously making a binary phase (A) that reacts to produce a hydrophilic boronic ester which is preferentially dissolved into the aqueous phase. Once the ester is formed the organic reaction solvent is selectively removed by capillary action (B) through port 3 and discarded. The remaining aqueous solution containing the boronic ester is pushed through to port 5 through (C), where an acidifying aqueous solution and a pure organic solvent are simultaneously injected (port 5) to hydrolyze the boronic ester to the hydrophobic boronic acid and extracted by the pure organic solvent (D). Once the extraction is complete the organic solvent containing the boronic acid is drawn off by capillary action (E) through port 7, while the remaining aqueous solvent exits port 6 and is discarded.

To carry out the complete reaction without quickly degrading the 3rd generation stainless steel chuck with concentrated hydrochloric acid during the second step hydrolysis of the boronic ester, we decided to add additional simple PFTE layers. The additional PTFE sandwiching layers act as a protecting layer to greatly reduce the contact of aqueous acid with the steel surface by being placed above and below the PFTE channel cut layer with 1mm cut port holes aligned with the steel chuck ports to allow infusion of liquids.

2.11 3rd Generation Chuck Design

The 3rd generation device flow network begins with a T-junction injection port 1(Figure 27) for an organic reaction solution (red) containing the boronic acid of interest and the aqueous basic solution (blue) of tripotassium phosphate and d-sorbitol. The combined phases move through the straight reactor channel along the path between port 1 and port 2 (Figure 27A) and forms the hydrophilic boronic ester adduct which dissolves into the aqueous solution. A microcapillary comb (Figure 27B) located before port 2 selectively removes organic solution (red) of the binary mixture into port 3 for collection, while the aqueous portion (blue) containing the boronic ester continues along the path between port 2 and port 4 (Figure 27C) which has a flow regulator inline. This channel connects with port 5, which is a 4 way connection for the addition of flow acidification solution (green) and fresh organic solvent (yellow). The aqueous acid hydrolyzes the hydrophilic boronic ester to the hydrophobic boronic acid, which is extracted by the fresh organic solvent inside of the second straight reactor channel (Figure 27D). Finally the binary mixture is separated using a second microcapillary comb (Figure 27E) to selectively remove the organic solvent (yellow) containing the boronic acid into port 7, while the aqueous solvent (green) is removed at port 6.

To achieve the depicted flow network (Figure 27), we designed a larger 316 stainless steel chuck (Figure 28), consisting of a pair of parallel smooth machined plates with machined fluid ports to provide easy fluid connections using UpChurch ¼-28 PEEK nuts and 1/16 tubing

ferrules.

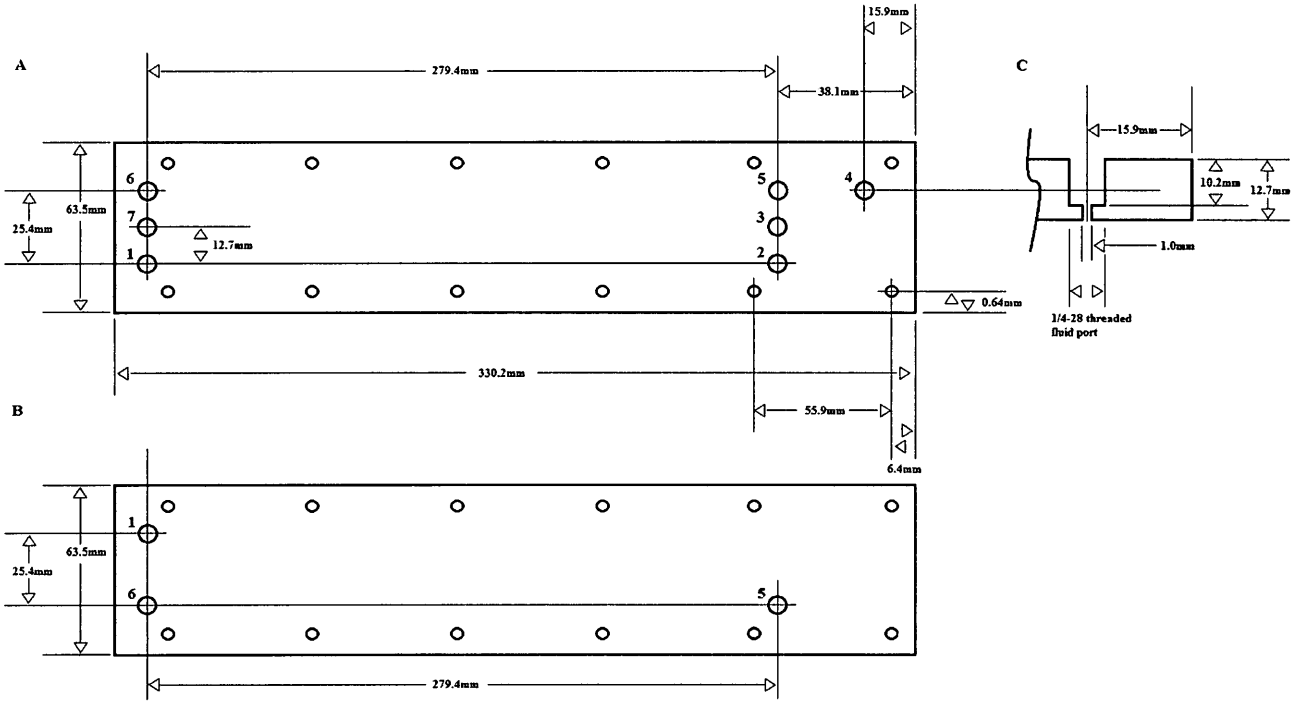

Figure 28: Measurements of the 316 stainless steel 3rd generation chuck to assemble our two-phase flow device. Numbered (1-7) (A and B) circles represent fluid ports (C). A) depicts the top surface of the upper plate, the smaller holes are unthreaded to accept the pressure sealing screws (35lbs.in torque). B) depicts the upper surface of the lower plate, where the smaller holes are threaded to accept the pressure sealing screws. C) depicts the general cross-section profile of the fluid ports (1/4-28 thread) for the tubing connects (numbered 1-7), with 1.0mm fluid ports leading bottom of the plates respectively to align with the laser cut PTFE channels once assembled.

2.12 3rd Generation PTFE Gasket Designs

The development of the 3rd generation PTFE gasket has gone through different iterations to address design problems, such as irreproducibility of flow behaviour, incomplete phase separation and incomplete recovery of pBA. The PTFE gaskets depicted in Figure 29 were our main designs for testing phase-separation of pure solvents, extract of the intermediate hydrophilic boronic ester and optimization of the basic and acidic tandem pBA recovery.

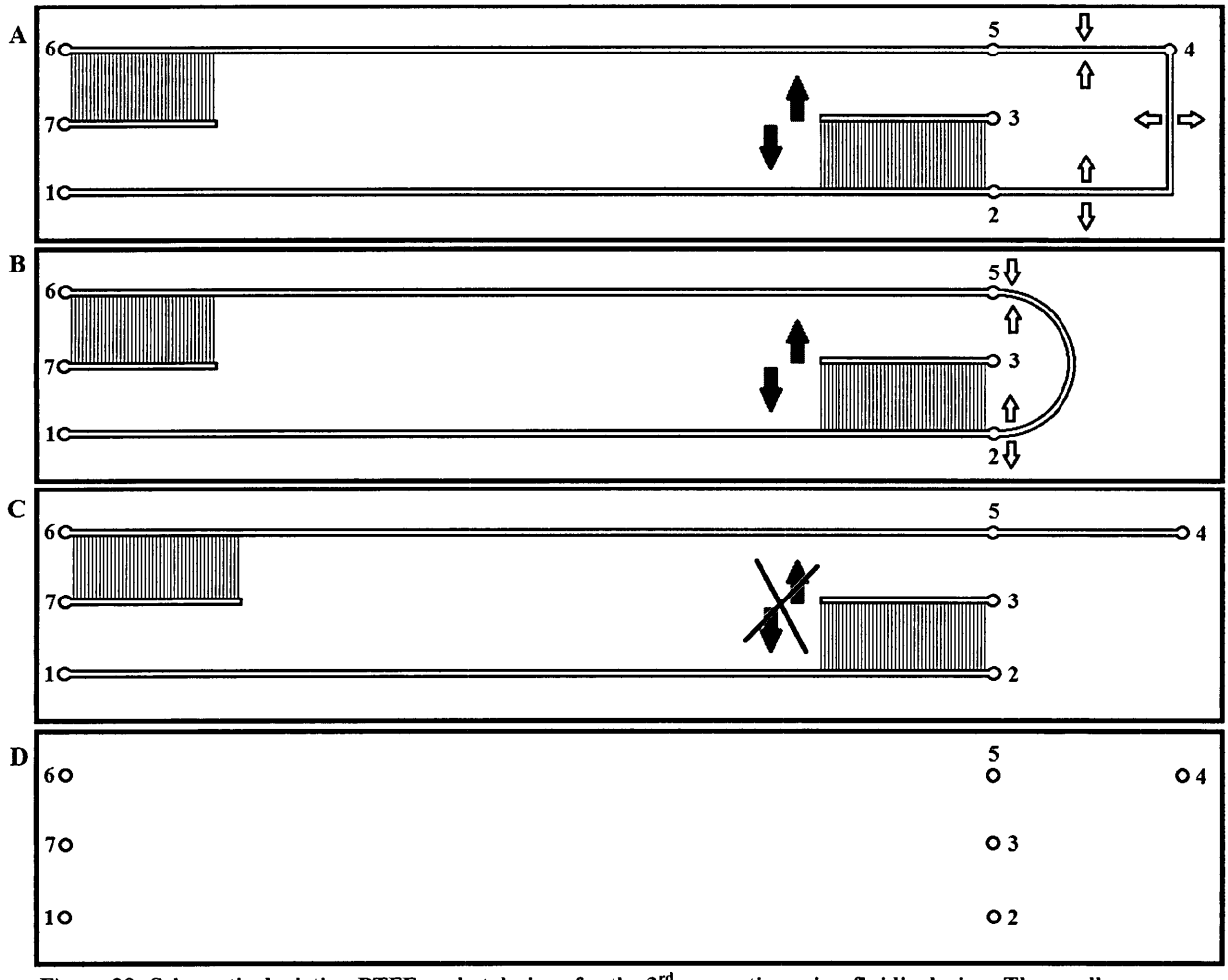

Figure 29: Schematic depicting PTFE gasket designs for the 3rd generation microfluidic device. The small vertically oriented lines represent 180 parallel micro-capillaries, the reverse side also has vertical engraved microcapillary channels totalling 360. The horizontal parallel lines represent two-phase reactor channels. The arrows represent unwanted movement of the central piece of PTFE which can move vertically (grey arrows), which pinch or widen the opposing channels near port 5, 2 and 4 (white arrows) causing unpredictable changes in flow behaviour. A) (Top) This design suffered from the movement of the inner portion of the gasket, where vertical movement in combination with the square edges of the microfluidic reaction channel resulted in erratic changes in pressure during operation and irreproducibility of results with the same design. B) (middle) The U-shaped design performed better than the previous gasket because experiments (Table 2) were successful but this design was also displayed irreproducibility between readjustments of the gasket. This was caused by pinching and widening of the channels between port 2 and 5. C) (bottom) The final design displays both stable flow separation behaviour and results are reproducible. Measurements are Port 1-2 281.7mm length, Port 5-6 281.7mm, all horizontal channels are 0.51mm depth and 0.51mm width. While the capillary channels are 13.2mm in length, with a parabolic profile of 0.26mm width and 0.26mm depth. D) Two of these sheets are fabricated to be placed between the channel layer PTFE and the steel chuck.

The testing of binary phase separation involved the use of ethyl acetate and distilled water to test the selective phase removal to determine appropriate flow rates for efficient separation. The separation of immiscible phases involves the injection of pure aqueous and organic solvent

(Figure 27, Port 1), mixing (Figure 27A), subsequent removal of the organic solvent using capillary action (Figure 27B), then injection of additional quantities of water and ethyl acetate (Figure 27, Port 5), is followed by a second capillary separation step (Figure 27E), where all eluted liquid volumes are measured from port 3, 6 and 7 (Figure 27) and compared to theoretical volumes.

The initial design PTFE gasket (Figure 29A) we tested had two 90 degree bends between (Figure 29A, Port 2) and (Figure 29A, Port 5) to connect the aqueous stream to the second extraction channel. This design was chosen for simplicity but proved to be a poor design choice considering our device materials and method of assembly. The testing of phase separation (Table 5) shows this PTFE design was a poor design since there was no reproducibility between experimental runs if the device is disassembled. Initially there were problems regarding the generation of fine emulsions of the collected phases and a lack of adequate phase separation at Port 3 (Figure 29A). This indicated that a sharp pressure drop in the system, which is a common method of microdroplet formation in MEMS systems.

Table 5: Volume recovery studies of first PTFE gasket (Figure 10A) for the 3rd generation device using pure hexanes and distilled water.

Entry	Total Flow Rate (1:1) (μL/min)		Recovered Ethyl Acetate Vol. Port 3 (mL)		Recovered H_2O Vol. Port 6 (mL)		Recovered Ethyl Acetate Vol. Port 7 (mL)	
	Port 1	Port 5	Meas. (%contam.)	Theor.	Meas. (%contam.)	Theor.	Meas. (%contam.)	Theor.
1a	140	-	3.5 (13%)	5.60	5.5 (2%)b	5.60	-	-
2a	140	-	1.30 (7%)	1.90	1.80 (25%)e	1.90	-	-
3c	140	17.4/69.7	1.00 (100%)	1.20	1.10 (20%)e	1.20	2.20 (5%)	1.20
4d	58.1	11.6/17.4	0.88(100%)	1.74	0.90 (5%)	2.44	1.35 (5%)	1.04
5	58.1	11.6/17.4	5.0 (50%)	-	3.0 (30%)	-	1.0 (0%)	-

a) entry 1 was a study of the efficiency of the PTFE gasket with ports 5, 6, and 7 blocked, while the aqueous stream was collected at port 2. b) a fine emulsion of ethyl acetate in water was observed. c) reversal of phase elution at port 3 (should be organic solvent but only water. d) only water eluted from port 3 but smaller sep. channels were fabricated ~0.25mm depth and ~0.25mm width. d) sep channels ~0.15mm depth and ~0.25mm width. e) emulsion observed. The PTFE gasket had channel lengths of Port 1 to Port 2 and Port 5 to Port 6 of 246mm, with a channel length abutting the capillary channels of 38.1mm, the length of channel between Port 2 and Port 5 was 70.0mm. The capillary channels are 12.5mm in length with a parabolic profile with ~0.25mm depth and ~0.5mm in width.

We believed the sharp pressure drop was occurring after Port 2 (Figure 29A) causing the generation of emulsions, where the binary phase passes the bend, it is broken up due to the angle and pressure drop experienced by the streams (Table 5, Entries 2 and 3). It was surmised that the device assembly caused unwanted distortion of the channels (grey and white arrows) (Figure 29A) causes the irreproducibility between runs (Table 5, Entries 1 and 2) and (Table 5, Entries 4 and 5). We also thought the capillary channels could be clogged or blocked prior to assembly, but clogging was not visually observed upon disassembly and sonication of the gaskets prior to assembly did not affect our results, with these inconsistent results a redesigned PTFE gasket was produced to hopefully mitigate these problems (Figure 29B).

The second PTFE design (Figure 29B) for the 3rd generation device was successfully deployed (Table 6) to test pure solvent phase separation similar to the phase-switching conditions for solvent removal. This design was first tested using distilled water and either ethyl acetate or hexanes as the model for phase-recovery, which were successful but still suffered some drawbacks, similar to the previous design with extremely poor or no phase separation at Port 3. The separation efficiency of this PTFE design did show some promise (Table 6, Entry 4, 5 and 7), achieving good separation of all three collected fractions from the device, while demonstrating that equal flow rate ratios of injected solutions are not required to achieve good phase separation (Table 6, Entry 7) with a small portion of the attempted experiments. Further experiments showed the operational window (flow rate range) was small, therefore we decided to attach a flow regulator to Port 3, in the hopes of obtaining better control of separation. This alteration seemed to make the problem of separation worse (Table 6, Entry 6) and reduced total volume flow through port 3 (Figure 27B). Another method was attempted to obtain better separation efficiencies in the U-shaped PTFE gasket (Table 6), where a fluid withdrawing syringe was attached to port 3 (Figure 27B). A representative experiment (Table 6, Entry 8) is provided and conducted at a variety of flow rates, but the production of negative pressure at Port 3 by withdrawing fluid does not work and typically unstable over long periods (15 minutes) producing poor separation of phases at Port 6 and 7, with contamination of approximately 20% to 35%. A further complication arose when the device was disassembled for cleaning, where numerous attempts at reassembly did not result in the reproduction of previous experiments. It was determined the irreproducibility was a result of PTFE gasket flexing, where pinching the flow channel connecting port 2 and port 5 (Figure 27C) greatly increases the backpressure in the reactor channel and separator comb (Figure 27A) effectively reversing the desired elution from organic solvents to aqueous at Port 3.

Table 6: Volume recovery studies of the U-shaped PTFE gasket (Figure 10B) 3rd generation device using pure hexanes and distilled water.

Entry	Total Flow Rate (1:1) (μL/min)		Recovered Hexane Vol. Port 3 (mL)		Recovered H_2O Vol. Port 6 (mL)		Recovered Hexane Vol. Port 7 (mL)	
	Port 1	Port 5	Meas. (%contam.)	Theor.	Meas. (%contam.)	Theor.	Meas. (%contam.)	Theor.
1	23.2	23.2	1.41 (0%)	3.48	5.42 (10%)	6.97	2.05 (0%)	3.48
2	116.3	23.2/5.8a	0.66 (0%)	1.22	1.10 (2%)	1.34	0.88 (12%)	0.48
3	232.6	23.2	0.32 (0%)	2.33	2.41 (20%)	2.56	1.06 (0%)	0.23
4*	46.4	23.2/11.6	2.00 (0%)	2.26	3.00 (0%)	4.51	1.10 (0%)	1.13
5*	46.4	23.2/11.6	1.50 (0%)	1.63	3.40 (0%)	3.26	0.60 (0%)	0.81
6b	46.4	46.4	0.55 (48%)	0.98	1.20 (0%)	1.95	0.03 (96%)	0.98
7c	46.4	11.6/23.2	0.95 (14%)	1.12	1.70 (0%)	1.67	0.95 (5%)	1.12
8	45	10/15d	1.6 (6%)	-	2.9 (3%)	-	2.6 (33%)	-

* flow regulators were located after ports 6 and 7 with 0.3" inner diameter tubing connections. The separation capillaries were parabolic in shape b) this experiment was preformed, then immediately started with flow rates of entry 6 and obtained identical separation values. c) after this entry the device was disassembled and reassembled 6 times and none of the previous experiments could be repeated. d) port 2 had a syringe pump set to withdraw fluid @ 15μL/min.

To address the problem of uncontrollable variation in channel width during assembly a new straight channel PTFE gasket design was made to eliminate any possible gasket flexing (Figure 29C). The redesigned PTFE gasket (Figure 29C) eliminated the internal channel connection and replaced it with external PEEK tubing, allowing for the incorporation of a flow regulator between port 2 and port 5 (Figure 27C) while halting PTFE gasket movement during assembly.

The added flow regulator between Port 2 and Port 5 (Figure 27C) was adopted because of a noticeable trend (Table 5 and 6) where the overall volume collection of ethyl acetate from port 3 was always much lower than predicted. The conditions of (Table 5 and 6) were then extended to our new design (Figure 29C), which displayed a similar tendency to have good phase separation

but poor overall solvent recovery (Table 7, Entry 1, 2 and 4) at least one fluid outlet port. Further experiments using pure solvent recovery tests demonstrated that adding a flow regulator between port 2 and port 5 (Figure 27C) remarkably increased phase separation and total recovered solvent volume (Table 7, Entry 6 and 7).

Table 7: Volume recovery studies of the straight line PTFE gasket (Figure 16C) 3rd generation device using pure hexanes and distilled water.

Entry	Flow Rate (H_2O:Hexane) (μL/min)		Recovered Hexane Vol. Port 3 (mL)		Recovered H_2O Vol. Port 6 (mL)		Recovered Hexane Vol. Port 7 (mL)	
	Port 1	Port 5	Meas. (%contam.)	Theor.	Meas. (%contam.)	Theor.	Meas. (%contam.)	Theor.
1a	20:20	20:20	1.19 (2%)	1.30	2.41 (0%)	2.60	1.18 (30%)	1.30
2a	20:20	10:10	0.91 (4%)	0.93	0.84 (0%)	1.39	0.22(76%)	0.46
3ac	20:20	10:20	0.66 (13%)	0.81	1.20 (8%)	1.22	0.48 (23%)	0.81
4ac	25:25	10:10	0.59 (0%)	1.16	1.70 (0%)	1.63	0.82 (18%)	0.47
5ac	25:25	20:20	0.74 (0%)	0.99	2.00 (2%)	1.77	0.80 (7%)	0.79
6b	20:20	20:20	0.76 (19%)	0.79	1.60 (0%)	1.58	0.70 (0%)	0.79
7b	25:25	25:25	1.25 (0%)	1.34	2.95 (0%)	2.67	1.10 (0%)	1.34

a) ports 6 and 7 have UpChurch flow rate regulators (P-446). b) in addition to port 6 and 7, there is another flow regulator (P-446) between port 2 and port 5 (Figure 8C). c) Port 2 during operation had the tendency to draw air into the device.

Once better solvent volume accounting and acceptable phase separation demonstrated by (Table 7, Entry 6 and 7), complete tandem phase-switching conditions using this design (Figure 29C) was performed for the optimization of inline recovery of pBA.

2.13 Investigation and Optimization of Phase-Switching Protocol for Microfluidic Application

The investigation involving the application of reaction protocols to microfluidic flow had a number of difficulties, which are easily handled with traditional batch methods but make reactions difficult or impossible under microflow conditions. The major concerns involved the generation of gases and particulates resulting in varying internal backpressure and blockage of channels respectively.

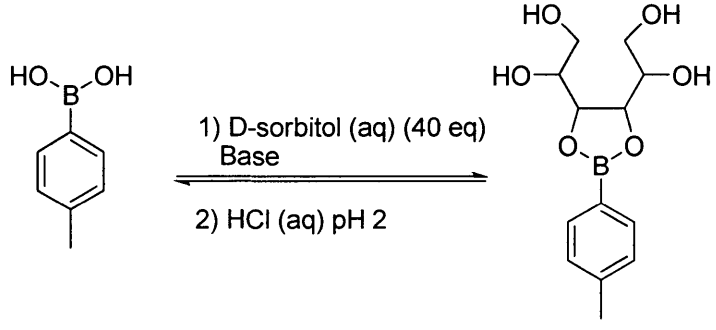

Table 8: Base screening of organic and aqueous bases for boronic ester formation in flow

Entry	Base	Equiv.	Recovery (%)[a]	pKa
1	Na_2CO_3	40	92[b]	9.3
2	Et_3N	40	63	10.7
3	DIPEA	40	70	35
4	$K_3PO_4 \cdot H_2O$	40	81	12.4
5	$K_3PO_4 \cdot H_2O$	80	94	12.4
6	$K_3PO_4 \cdot H_2O$	60	>95	12.4

a) boronic acid recovery determined using anisole internal standard (^{1}H-NMR). b) standard condition using Dennis Hall protocol.

The initial phase-switching conditions developed by Hall et al. used of d-sorbitol (1.0M) as the ester forming adduct and aqueous sodium carbonate (1.0M) to initiate the boronic ester formation and subsequent extraction, which is in turn acidified with (6.0M) aqueous hydrochloric acid to reform the boronic acid, producing carbon dioxide as a by-product. To eliminate carbon

dioxide generation from acidification a number of organic and aqueous bases (Table 8) with similar pKa to sodium carbonate were screened. Initial experiments utilizing hindered amine bases (Table 8, Entries 2,3) yielded poor recovery results, this may occur because of a slow equilibrium process or the base must be present in the aqueous phase to affect hydrophilic ester formation. The use and optimization of tripotassium phosphate is comparable to sodium carbonate for attaining the recovered boronic acid (Table 8, Entries 4-6) 95%. Under the standard batch conditions as well as preliminary flow experiments (Table 9) using the first step involving ester formation and extraction, where it was determined that tripotassium phosphate was suitable by obtaining similar results in comparison to previous conditions (Table 9, Entry 8).

Several tests were performed to determine whether aqueous $K_3PO_4 \cdot H_2O$ base performed as efficiently as sodium carbonate for fast formation and extraction of hydrophilic boronic esters in flow using similar flow conditions. These tests (Table 9) were performed using the 3rd generation chucks (Figure 28) and PTFE gasket design (Figure 29C) with Port 2 and 3 acting as outlet ports to obtain aqueous and organic solutions respectively by blocking all further downstream ports. These experiments show that our conditions (Table 9, Entry 8) with a residence time of 41 seconds achieved 95% recovery.

Table 9: Recovery of p-tolyl boronic acid using flow conditions in (Figure 26C) 3rd Generation flow device for esterification using $K_3PO_4.H_2O$ with batch acidic hydrolysis and extraction.

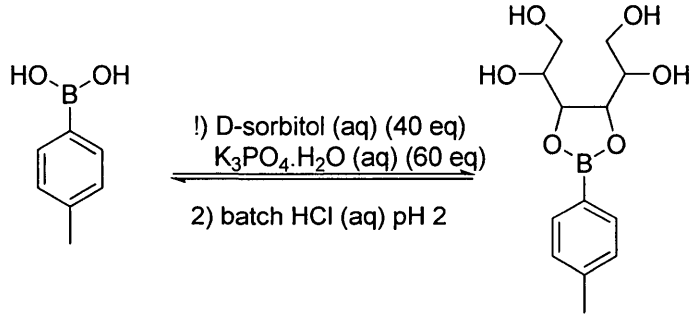

Entry	Width (mm)	Aspect Ratio	Residence Time (s)	Total Flow Rate (uL/min)	Recovery %[e]
1	-	-	-	-	92
2a	0.254	0.85	61	40	90
3b	0.254	0.85	61	40	72
4c	0.254	0.85	82	30	53
5d	-	-	-	-	95
6	0.254	0.85	27	100	65
7	0.254	0.85	35	70	82
8	0.254	0.85	41	60	95

* separation of phases at outlet using capillary action were achieved with 95% efficiency for the first step of our phase switch conditions. (a) Total collection time (1hrs). (b) total collection time (8hrs). (c) total collection time (11hrs). (d) control experiment batch time (8hrs). (e) recovery % determined using internal standard by proton NMR +/- 5%.

For comparison (Table 9, Entry 1) represents the initial batch conditions optimized by Hall with a recovery of 92% using sodium carbonate, while (Table 9, Entry 5) are our conditions using potassium phosphate monohydrate obtaining similar results of 95% using identical shake flask methods. Difficulties arose since the collected samples from the flow reaction and extraction resided in the collection vial for long periods of time, which seemed to result in decreased recovery for longer flow times (Table 9, Entry 2) from 90% to (Table 9, Entry 3) 72%

to (Table 9, Entry 4) 53% as collection time increased. This could have resulted from the slow back extraction of the sugar-based hydrophilic boronic ester from the aqueous solution into the contaminating organic phase as the hydrophobic methoxy boronic ester. The unwanted hydrophilic extraction is initiated by the basic hydrolysis of the ethyl acetate solvent to acetic acid and ethanol, which can slowly displace d-sorbitol based on pKa. We then optimized flow conditions to obtain 95% recovery with a 41 second residence time and a total flow rate of 60μL/min (Table 9, Entry 8), where the acidic hydrolyzing step is performed under batch conditions.

The final optimization of the phase-switching process in the 3rd generation device involved the inline hydrolysis as the final acidification step to complete the tandem reaction-extraction process and determine the optimal flow parameters for overall maximum material recovery. A number of problems arose attempting to implement the complete tandem phase-switching reaction, such as clogging issues which hindered long running flows of over 1 hour, and incomplete final extraction of the hydrolyzed product.

Table 10: p-tolyl boronic acid recovery experiments using our optimized conditions with 3rd Generation flow device using PTFE (Figure 26C) design.

Entry	Flow Rate (Aq:Org) (μL/min)		Recovered Hexane Vol. Port 3 (mL)		Recovered Aq. Vol. Port 6 (mL)		Recovered Org. Vol. Port 7 (mL)	
	Port 1	Port 5	Meas. Vol. (Exp. Vol)	Recov.%	Meas. Vol. (Exp. Vol)	Recov.%	Meas. Vol. (Exp. Vol)	Recov.%
1	23.2:23.2	23.2:23.2	1.98 (0)	0	4.39 (9)	25	1.34 (0)	54
2	29:29	29:29	2.13 (0)	0	5.00 (0)	24	1.44 (0)	56
3	29:29	17.4:29	1.96 (0)	0	3.63 (4)	15	1.74 (0)	70
4	25:25	20:20	1.05 (0)	0	2.24 (0)	11	0.68(0)	75
5	15:15	15:15	1.90 (3)	0	4.37 (1)	10	2.38(0)	75
6*a	25:25	10:35	1.83 (0)	0	2.60 (0)	0	2.56(0)	58
7*a	25:25	10:35	-	0	-	7	-	53
8bc	20:20	10:30	-	0	-	15	-	58
9d	20:20	10:30	-	0	-	24	-	57
10e	15:15	15:20	-	0	-	4	-	45

conditions: 0.025M p-tolyl boronic acid dissolved in EtOAc, 1.0M D-sorbitol and 1.5M potassium phosphate monohydrate dissolved in distilled water, pure EtOAc extraction solvent, aqueous 4.51M HCl. a) 9.02M HCl b) 3.6M HCl (results in neutral pH collected solutions) c) fluorolube coating on interior of side of assembled steel plates as protecting layer to stop flow of acid between PTFE layers results in flow times of 5hours with no clogging of system. d) HCl (aq) 7.0M e) HCl (aq) 4.51M.

The final optimization of flow conditions for phase-switching of p-tolyl boronic acid in our final 3rd generation device with the best performing PTFE channel design (Figure 29C) proved to be more difficult than initial work performed for ester formation. Difficulties arose from the clogging of the channels close to the outlet port 6 and 7 (Figure 27E) resulting in sudden loss of phase separation but this would be accompanied by the precipitation of needle-shaped crystals in the collection vials. These crystals are the most likely cause of our clogging issues but

there is also the issue of leakage which became apparent that could be contributing to poor recoveries, channel clogging and steel chuck degradation. Experiments conducted for the complete tandem reaction demonstrated a strange inadequacy of our design which only became apparent once a larger range of flow rates and product recoveries was performed. Initially, we chose a moderate flow rate to test our conditions (Table 10, Entry 1) which gave a 100% removal of the boronic acid from ethyl acetate injected into port 1 (Figure 27A). This is an efficient extraction where even doubling flow rate to 30μL/min produced 100% removal of the substrate. This is opposed to the organic extraction of the hydrolyzed boronic acid, where flow rate did not correlate to extraction efficiency (Table 10, Entry 5) versus (Table 10, Entry 10). The device showed promise (Table 10, Entries 1-4) where it seemed there was a correlation between flow rate and recovery of the substrate under our standard conditions but it later became apparent when we tried to optimize our flow conditions the system performed poorly (Table 10, 6-10). The reactions performed for the optimization of the system were initially performed over short periods of time (approx. 1.5hours) to collect enough material for analysis because the longer flow times resulted in port blockages (ports 6 or 7). The clogging issue was addressed by applying fluorolube grease to adhere the protective PTFE sheet to the chuck, this worked because acid was leaking inside of the chuck and corroding the steel which clogged the downstream ports. By applying fluorolube to potentially prevent solvent leaking internally but almost immediately it was washed away completely by the organic solvent which seemed to wick through the different PTFE layers causing corrosion and loss of boronic acid substrate. We also observed the build-up of solid pBA between the PTFE protecting layer and the steel chuck near outlets (ports 6 and 7), so we believe it is the cause of lower than expected mass recoveries (Table 10, Entries 6-10). Although our design was flawed because of the multiple PTFE layer design where organic

solvent can leak internally due to low viscosity and surface tension, single layer designs would better serve for the flow network.

3.0 Conclusion

The successful design and implementation of the 3rd generation device using an optimized PTFE channel design to facilitate the conversion of a batch phase-switching purification scheme into an integrated flow format only afforded purified product in low to moderate recoveries. This project proved to be difficult since the two-phase chemistry involved is difficult to predict once introduced into microreactors which is also greatly influenced by any changes, abnormalities or unknown flaws in the reactor design. The final system proved that using boronic acid functionalities as a "homogeneous solid phase" purification to draw the molecule of interest selectively from a reaction mixture is possible using a simpler single layer design to prevent leakage of solvent and can be incorporated as an intermediate unit operation between separate transformations and analysis steps.

A future direction of the present work is the use of other types of phase switching tags and extraction techniques for inline purification of substrates. This would include developing fluorous tagging strategies,[97] and other selective extraction techniques for use in our generalized flow reactor. Another direction would develop a single layer device using a similar flow network to facilitate our phase-switching reaction using highly chemically resistant materials such as continuous blocks of engraved PTFE, with tapped ports.

References

[1] Baumann, M.; Baxendale, I. R.; Ley, S.V.; Smith, C. D.; Tranmer, G. K.; *Org. Lett.* **2006**, 23, 5231-5234.
[2] Yoshida, J.; Kim, H.; Nagaki, A.; *ChemSusChem.* **2011**, 4, 331-340.
[3] Roberge, D. M.; Ducry, L.; Bieler, N.; Cretton, P.; Zimmermann, B. *Chem. Eng. Technol.* **2005**, 28, 318-323.
[4] Nikoubashman, A.; Kahla, G.; Likos, C. N. *Soft Matter.* **2012**, 8, 4121-4131.
[5] Genovese, D.; Sprakel, J.; *Soft Matter.* **2011**, 7, 3889-3896.
[6] Manz, A. *J. Chromatogr.* **1992**, 593, 253-258.
[7] Hornung, C. H.; Mackley, M. R.; Baxendale, I. R.; Steven, L. V. *Org. Proc. Res. Dev.* **2007**, 11, 399-405.
[8] Bogojevic, D.; Chamberlain, M. D.; Barbulovic-Nad, I.; Wheeler, A. R. *Lab on a Chip.* **2012**, 12, 627-634.
[9] Ainla, A.; Jansson, E. T.; Stepanyants, N.; Orwar, O.; Jesorka, A. *Anal. Chem.* **2010**, 82, 4529-4536.
[10] Guenther, A.; Yasotharan, S.; Vagaon, A. *Lab on a Chip.* **2010**, 10, 2341-2349.
[11] Yanagisawa, N.; Mecham, J. O.; Corcoran, R. C.; Dutta, D.; *Anal. Bioanal. Chem.* **2011**, 401, 1173–1181.
[12] Bardin, D.; Martz, T. D.; Sheeran, P. S.; Shih, R.; Dayton, P. A.; Lee, A. P. *Lab on a Chip.* **2011**, 11, 3990-3998.
[13] Yuen, P. *Lab on a Chip.* **2008**, 8, 1374-1378.
[14] Mitra, A.; Thareja, R. K. *J. Mat. Sci.* **1999**, 34, 615– 619.
[15] Yanqiang, Y.; Shufeng, W.; Zhaoyong, S.; Dana, D. D. *Appl. Phys. Lett.* **2004**, 85, 1493-1496.
[16] Mu, X.; Liang, Q.; Hu, P. *Lab on a Chip.* **2009**, 9, 1994-1996.
[17] Jinno, N.; Hashimoto, M. *Anal. Sci.* **2009**, 25, 145-147.
[18] Guriyanonva, S.; Semin, B. *Microfluid. Nanofluid.* **2010**, 8, 653-663.
[19] Tenstad, E.; Tourovskaia, A. *Lab on a Chip.* **2010**, 10, 1401-1409.
[20] He, P.; Greenway, G.; Haswell, S. *Microfluid. Nanofluid.* **2010**, 8, 565-573.
[21] Dae-Hun, J.; Jae, K. M.; Do, Y. N.; Kwang, H. K.; Jong-Hyun, L. *Nuc. Instr. Meth. Phys. Res.* **2011**, 652, 846–849.
[22] McAuley, S. A.; Ashraf, H.; Atabo, L.; Chambers, A.; Hall, S.; Hopkins, J.; Nicholls, G. *J. Phys. D: Appl. Phys.* **2001**, 34, 2769–2774.
[23] Singleton, L. *J. Photopolym. Sci. Technol.* **2003**, 16, 413-421.
[24] Joye, C. D.; Calame, J. F.; Nguyen, K. T.; Garven, M. *J. Micromech. Microeng.* **2012**, 22, 11.
[25] Sollier, E.; Murray, C.; Maoddi, P.; Di Carlo, D. *Lab Chip.* **2011**, 11, 3752-3765.
[26] Kuper, S.; Stuke, M. *Appl. Phys. Lett.* **1989**, 54, 4-6.
[27] Kuhn, S.; Noel, T.; Gu, L.; Heidera, P. L.; Jensen, K. F. *Lab Chip.* **2011**, 11, 2488–2492.
[28] Kuhn, S.; Hartman, R. L.; Sultana, M.; Nagy, K. D.; Marre, S.; Jensen, K. F. *Langmuir.* **2011**, 27, 6519–6527.
[29] Duffy, D. C.; Gillis, H. L.; Lin, J.; Sheppard, N. F.; Kellogg, G. *J. Anal. Chem.* **1999**, 20, 4669-4678.
[30] Breadmore, M. C. *J. Chromat. A.* **2012**, 1221, 42–55.
[31] Wang, W.; Zhoua, F.; Zhaoa, L.; Zhang, J.; Zhua, J. *J. Chromat. A.* **2007**, 1170, 1–8; Gaudioso, J.; Craighead, H. G. *J. Chromat. A.* **2002**, 971, 249–253.
[32] Demirci, U. *JMEMS.* **2006**, 15, 957-966.
[33] Darhuber, A. A.; Troian, S. M. *Annu. Rev. Fluid Mech.* **2005**, 37, 425–455.
[34] Pollack, M. G.; Fair, R. B.; Shenderov, A. D. *Appl. Phys. Lett.* **2000**, 11, 1725-1726.
[35] Vetcha, S.; Wilkins, E.; Yates, T.; Hjelle, B. *Talanta.* 2002, 3, 517-528.
[36] Dittmer, W. U.; Evers, T. H.; Hardeman, W. M.; Huijnen, W.; Kamps, R.; Kievit, P.; Neijzen, J. H. M.; Nieuwenhuis, J. H.; Sijbers, M. J. J.; Dekkers, D. W. C.; Hefti, M. H.; Martens, M. F. W. C. *Clinica Chimica Acta.* **2010**, 411, 868–873.

[37] Romana, G. T.; Kennedy, R. T. *J. Chromat. A.* **2007**, 1168, 170–188.
[38] Bruus, Henrik. *Theoretical Microfluidics.* Oxford : Oxford University Press, 2007pg 51
[39] Bruus, Henrik. *Theoretical Microfluidics.* Oxford : Oxford University Press, 2007pg 26
[40] Kumar, C. S. *Microfluidic Devices in Nanotechnology,* Wiley-VCH, **2010**, 73.
[41] Bruus, Henrik. *Theoretical Microfluidics.* Oxford : Oxford University Press, 2007pg 80
[42] Kumar, C. S. *Microfluidic Devices in Nanotechnology,* Wiley-VCH, **2010**, 75.
[43] Kumar, C. S. *Microfluidic Devices in Nanotechnology,* Wiley-VCH, **2010**, 74.
[44] Choi, C.; Yu, D. I.; Kim, M. *Exp. Therm. Fluid. Sci.* **2011**, 6, 1086–1096.
[45] Aota, A.; Nonaka, M.; Hibara, A.;Kitamori, T. *Angew. Chem. Int. Ed.* **2007**, 46, 878 –880.
[46] Sugiura, S.; Nakajima, M.; Seki, M. *Langmuir.* **2002**, 18, 5708–5712.
[47] Anna, S. L.; Bontoux, N.; Stone, H. A. *Appl. Phys. Lett.* **2003**, 82, 364-366.
[48] Garstecki, P.; Fuerstman, M. J.; Stone, H. A.; Whitesides, G. M. *Lab on a Chip*, **2006**, 6, 437–446.
[49] Funada, T.; Joseph, D. D. *J. Fluid. Mech.* **2001**, 445, 263–283.
[50] Song, H.; Tice, J.; Ismagilov, R. *Angew. Chem., Int. Ed.* **2003**, 42, 768–772.
[51] Xia, H. M.; Wan, S. Y. M.; Shu, C.; Chew, Y. T. *Lab on a Chip*, **2005**, 5, 748-755.
[52] Song, H.; Tice, J. D.; Ismagilov, R. F. *Angew. Chem. Int. Ed.* **2003**, 42, 768-772.
[53] Guenther, A.; Jensen, K. F. *Lab on a Chip.* **2006**, *6*, 1487-1503.
[54] Lewpiriyawong, N.; Kandaswamy, K.; Yang, C.; Ivanov, V.; Stocker, R. *Anal. Chem.* **2011**, 83, 9579–9585.
[55] Yung, C. W.; Fiering, J.; Mueller, A. J.; Ingber, D. E. *Lab on a Chip.* **2009**, 9, 1171–1177.
[56]Guldiken, R.; Jo, M. C.; Gallant, N. D.; Demirci, U.; Zhe, J. *Sensors.* **2012**, 12, 905-922.
[57] Nagai, H.; Miwa, N.; Segawa, M.; Wakida, S.; Chayama, K. *J. Appl. Phys.* **2009**, 105, 102015.
[58] Huh, Y. S.; Park, T. J.; Yang, K.; Lee, E. Z.; Hong, Y. K.; Lee, S. Y.; Kim, D. H.; Hong, W. H. *Ultramicroscopy*. 2008, **108**, 1365-1370.
[59] Tanaka, K.; Motomatsu, S.; Koyama, K.; Fukase, K. *Tet. Lett.* **2008**, 49, 2010–2012.
[60] Miyazaki, M.; Yamaguchi, Y.; Honda, T.; Maeda, H. *The Open Chemical Engineering Journal.* **2011**, 5, 13-17.
[61] Toh, G. M.; Yanagisawa, N.; Corcoran, R. C.; Dutta, D. *Microfluid. Nanofluid.* **2010**, 9, 1135–1141.
[62] Negrete, A.; Ling, T. C.; Lyddiatt, A. *J. Chromatography. B.* **2007**, 854, 13-19.
[63] Maruyama, T.; Kaji, T.; Ohkawa, T.; Sotowa, K.; Matsushita, H.;Kubota, F.; Kamiya, N.; Kusakabe, K.; Goto, M. *Analyst.* 2004, **129**, 1008-1013.
[64] Gunther, A.; Jhunjhunwala, M.; Thalmann, M.; Schmidt, M. A.; Jensen, K. F. *Langmuir.* **2005**, 21, 1547-1555.
[65] Tagawa, T.; Aljbour, S.; Matouq, M.; Yamada, H. *Chem. Eng. Sci.* **2007**, 62, 5123 – 5126.
[66] Ju, W.; Fu, L.; Yang, R.; Lee, C. *Lab on a Chip.* **2012**, 12, 622-626.
[67] Angelescu, D. E.; Mercier, B.; Siess, D.; Schroeder, R. *Anal. Chem.* **2010**, 82, 2412–2420.
[68] Gunther, A.; Jhunjhunwala, M.; Thalmann, M.; Schmidt, M. A.; Jensen, K. F. *Langmuir.* **2005**, 21, 1547-1555.
[69] Kralj, J. G.; Sahoo, H. R.; Jensen, K. F. *Lab on a Chip.* **2007**, 7, 256–263.
[70] Extrand, C. W.; Moon, S. I. *Langmuir.* **2012**, 25, 3503-3509.
[71] Daley, A. B.; Oleschuk, R. D. *Journal of Chromatography A.* **2009**, 1216, 772–780.
[72] Lehmler, H. J.; Telu, S.; Vyas, S. M.; Shaikh, N. S.; Rankin, S. E.; Knutson, B. L.; Parkin, S. *Tetrahedron.* **2010**, 66, 2561–2569.
[73] Reid, C. S.; Zhang, Y.; Li, C. *Org. Biomol. Chem.* **2007**, 5, 3589–3591.
[74] Goto, K.; Mizuno, M. *Tetrahedron Let.* **2010**, 51, 6539–6541.
[75] Tzschucke, C. C.; Bannwarth, W. *Helvetica Chimica Acta.* **2004**, 87, 2882-2889.
[76] Siu, J.; Baxendale, I. R.; Lewthwaite, R. A.; Ley, S. V. *Org. Biomol. Chem.* **2005**, 3, 3140–3160.
[77] Desset, S. L.; Cole-Hamilton, D. J. *Angew. Chem. Int. Ed.* **2009**, 48, 1472 –1474.
[78] Subner, M.; Plenio, H. *Angew. Chem. Int. Ed.* **2005**, 44, 6885–6888.
[79] Minati, L.; Biffis, A. *Chem. Commun.* **2005**, 8, 1034–1036.

[80] Mothana, S.; Chahal, N.; Vanneste, S.; Hall, D. G. *J. Comb. Chem.* **2007**, 9, 193-196.
[81] Mothana, S.; Grassot, J.; Hall, D. G. *Angew. Chem. Int. Ed.* **2010**, 49, 2883-2887.
[82] O'Brien, C. J.; Assen, E.; Kantchev, B.; Valente, C.; Hadei, N.; Chass, G. A.; Lough, A.; Hopkinson, A. C.; Organ, M. G. *Chem. Eur. J.* **2006**, 12, 4743-4748.
[83] Hall, D.; *Boronic acids: Preparation and Applications in Organic Synthesis and Medicine*, Wiley-VCH, **2005**, 55.
[84] Zhong, Z.; Anslyn, E. V. *J. Am. Chem. Soc.* **2002**, 124, 9014-9015.
[85] Chen, M.; Wang, J.; Chai, Z.; You, C.; Lei, A. *Adv. Synth. Catal.* **2012**, 354, 341 – 346.
[86] Inamoto, K.; Hasegawa, C.; Hiroya, K.; Kondo, Y.; Osako, T.; Uozumi, Y.; Doi, T. *Chem. Commun.* **2012**, 48, 2912–2914.
[87] Kuivila, H.G.; Keough, A.H.; Soboczenski, E.J.; *J. Org. Chem.* **1954**, 8, 780-783.
[88] Baker, S.J.; Tomshob, J.W.; Benkovic, S.J.; *Chem. Soc. Rev.* **2011**, 40, 4279–4285.
[89] Albers, H.; Hendrick, L.J.; Van Tol, R.; Hausmann, J.; Perrakis, A.; Ovaa, H. *J. Med. Chem.* **2011**, 54, 4619–4626.
[90] Matsumoto, A.; Yoshida, R.; Kataoka, K. *Biomacromolecules*. **2004**, 5, 1038-1045.
[91] Larkin, J.D.; Frimat, A.F.; Fyles, T.M.; Flower, S.E.; James, T.D. *New J. Chem.* **2010**, 34, 2922–2931.
[92] Hoeg-Jensen, T.; Ridderberg, S.; Havelund, S.; Schaffer, L.; Balschmidt, P.; Jonassen, I.; Vedsø, P.; Olesen, P.H.; Markussen, J. *J. Peptide Sci.* **2005**, 11, 339–346.
[93] Yang, W.; Fan, H.; Gao, X.; Gao, S.; Vardhan, V.; Karnati, R.; Ni, W.; Hooks, W.B.; Carson, J.; Weston, B.; Wang, B. *Chemistry & Biology*. **2004**, 11, 439–448.
[94]. Lorand, J.P.; Edwards, J.O. *J. Org. Chem.* **1959**, *24*, 769.
[95] Mothana, S.; Grassot, J. M.; Hall, D.G. *Angew. Chem. Int. Ed.* **2010**, 49, 2883.
[96] Wilson, D.; Konermann, L. *Anal. Chem.* **2005**, 77, 6887-6894.
[97] Horhant, D.; Le Lamer, A.; Boustie, J.; Uriac, P.; Gouault, N. *Tetrahedron Letters.* **2007**, 48, 6031.

4.0 Appendix

4.1 Theoretical p-tolyl boronic acid calculations of diffusion time

Sample calculation of diffusion coefficient for p-tolylboronic acid

We estimated the (R_h) Hydrodynamic radii or Stokes radius as 2 angstroms, where larger proteins are ~6-8 Angstroms, which over estimates the size of the molecule making calculations larger than expected. The Stokes radius estimates a hard sphere that diffuses at the same rate as a molecule of roughly the same size.

(hydrodynamic radii) R_h = 2E-10m

(temperature) T=24°C (297K)

(Boltzmanns constant) k_b = (1.3806E-23kg m^2 s^{-2} K^{-1})

(kinematic viscosity of ethyl acetate) η= 0.000426kg $m^{-1}s^{-1}$

$$D = \frac{k_b T}{6\pi\eta R_h}$$

$$D = \frac{(1.3806E-23 kgm^2 s^{-2} K^{-1})(297K)}{6\pi(0.000426 kgm^{-1} s^{-1})(2E-10m)}$$

$$D = 2.55E-9 m^2 s^{-1}$$

Therefore the estimated diffusion coefficient for p-tolylboronic acid is 2.55E-9m^2s^{-1}.

Sample calculation of log P determination of p-tolylboronic acid

initial mass = 97.8mg

volume of EthOAc = 10.0mL

volume of water = 10.0mL

final mass = 94.4mg

$$M_{org} = \frac{94.4mg}{10mL} = 9.44g/L$$

$$M_{water} = \frac{97.8mg - 94.4mg}{10mL} = 0.34g/L$$

$$LogP = \log\left(\frac{M_{org}}{M_{water}}\right) = \log\left(\frac{9.44g/L}{0.34g/L}\right) = 1.44$$

Calculation of diffusion time of p-tolylboronic acid through EtOAC across a 254μm channel width

This calculation describes the diffusion of the substrate through the ethyl acetate phase and assumes the molecule undergoes esterification faster than the rate of diffusion and is immediately removed from the organic phase into the aqueous phase. Also since the channel is occupied by two phases, where each are assumed to inhabit half of the characteristic width of 254 μm, we assume the entire width so underestimation of diffusion time does not occur.

(smallest channel dimension) w = 0.00038m

(diffusion coefficient) D = 2.55E-9m^2 s^{-1}

$$T_{diff} = \frac{\left(\frac{2}{3}w\right)^2}{D}$$

$$T_{diff} = \frac{\left(\frac{4}{9}\right)(380E-6m)^2}{2.55E-9m^2s^{-1}}$$

$$T_{diff} = 25.2s$$

Renoylds number calculation for the microfluidic flow in the 3rd generation device

(channel area) A = lw = (510E-6 m)(380E-6m) = 1.79E-7m^2

(channel length) L = 0.31m

(total flow rate) Q = 120μL/min = 2.00E-9m^3/s

(kinetic viscosity of water) η = 0.001004 m^2s^{-1}

$$\mathrm{Re} = \frac{QL}{\nu A}$$

$$\mathrm{Re} = \frac{(2.00E-9m^3s^{-1})(0.31m)}{(5.59E-8m^2)(1.004E-3kgm^2s^{-1})}$$

$$\mathrm{Re} = 3.2$$

3rd Generation General Fabrication and Assembly Instructions

The PTFE film is laser ablated using a (Versalaser 2.30) with a 30W laser source, while the PTFE was obtained from CSHyde in 12" wide rolls in varying thickness (0.003", 0.010", 0.015", 0.020", 0.050", 0.100" with a tolerance of 0.001"). The sheets were then rough cut using a sharp razor blade into the outline of the gasket, then the PTFE rough cut is aligned with the cutting area guides and double sided adhesive is used to reversibily adhere the entire area of PTFE to the cutting surface (to prevent warping from the laser heat). Then using Corel Draw 9, a suitable fluid design is made which aligns the fluid ports located on the inner surface of the stainless steel chucks, aligning the ports requires either making the fluidic port holes 2-3mm in diameter in the PTFE surface or using small guage copper wire for aligning the PTFE channels with the steel chuck fluid ports. The screws for applying pressure and sealing the PTFE channels are 4mm socket head screw caps (#10 – 32 X 1) and are finger tightened in order of 1-12 (diagram 1). Once finger tightened a torque wrench is used to tighten each bolt in order of 1 through 12 by an 1/8 of a turn (35lbs.in torque). This ensures there is no over tightening (strip the bolts, crush the channels, increase PTFE creep) or under tighten (leaks).

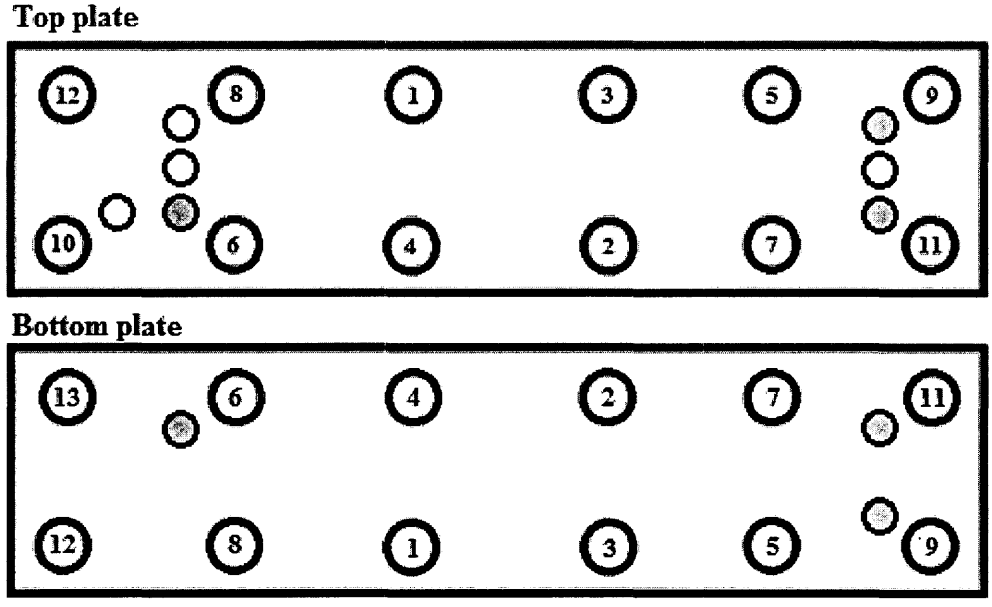

Figure 30: Torque screw diagram for 3rd generation flow device. The larger numbered circles represent the top plate screw holes which are not threaded, while the bottom plate screw holes are threaded so pressure sealing is achieved through compression of the plates upon the PTFE gasket. The above diagram also shows the mirrored numbering of the top and bottom plates denoting the arrangement of the plates once assembled. The unlabelled smaller circles represent the ¼-28 fluid ports, while the grey color ports denotes fluid port overlap.

Once the device has been assembled and appropriate fluid connections are made to reagent reservoirs, such as a dual syringe pump (Harvard Pump 11). All fluid connections were made using UpChurch Scientific standard ¼-28 PEEK nuts and 1/16" ferrules coupled with clear PEEK tubing with an outer diameter tubing and internal diameter of 0.02 inches. Fluid tubing lengths used were always minimized and all had equal lengths. Flow regulators from UpChurch Scientific P-446 are then fixed at the outlet port 6 and outlet port 7 corresponding to aqueous and organic elution ports respectively. The PEEK nuts and ferrules must be tightly wrapped with Teflon tape to prevent leakage through the ports and then finger tightened into place. Then a dual syringe pump (Harvard Pump 11) is used to inject the initial boronic acid solution and basic aqueous media, where both are connected by a tee-junction to port 1. Then a second dual syringe pump (Harvard Pump 11) fitted with a syringe of fresh organic solvent and a separate syringe of aqueous acidic media are both connected to port 5 using a tee-junction. While the connection

from port 2 to port 4 is bridged using two short 1.5" lengths of PEEK tubing connected with a flow regulator (P-446).

General Experimental Procedure

Once the device is assembled with all of the accompanying tubing the system must be purged of all air or water before any experimentation can commence. The purging is accomplished using the fresh organic solvent syringe located at port 5, which is generally overfilled with EtOAc, which is used to purge the system using typical system flow rates (10-30μL/min). The pair of 10mL (plastic syringes) were loaded with prepared organic and aqueous solutions, 0.025M p-tolyl boronic acid dissolved in EtOAc and 1.0M D-sorbitol and 1.5M potassium phosphate monohydrate dissolved in distilled water, prepared using 10mL volumetric flasks and connected to port 1. While in identical syringes (10mL) were filled with pure EtOAc and aqueous 4.51M HCl prepared from a stock solution. The syringes at port 1would begin pumping and after 2 minutes the syringes at port 5 would begin pumping. After 10 minutes of continuous operation the head of the flow which eluted would be discarded and collection time would commence for approximately 6 hours to collect the boronic acid product with conversions between 50-75%. After collection of the phase-separated solutions in separate vials the volume of liquids would be measured using either a 10mL graduated cylinder or a 1mL syringe for smaller volumes. Then the solutions would be washed with 10-15mL of distilled water in a separatory funnel to remove remaining salts and 10-15mL of brine and vacuum dried and dissolved into d6-DMSO and anisole was used as an internal standard to determine recovery by proton NMR thorough comparison of methyl and methoxy peak integration and compared to known literature NMR spectra (Hall et al).

Optical Images of Laser Cut PTFE Channels

Optical photos of microchannels in 0.51mm thick Teflon film (1mm=60 graduations). Left panel is a top down photo of the microchannel. Right panel is a profile image of the same microchannels.

Entry	Laser Setting *	Laser Power (%)	Number of laser passes	Theoretical width (mm)	Measured Width (mm)	Measured Depth (mm)
A	V, P, A	0	1	0.05	0.26	0.52
B	R, P, MSDE	50	3	0.05	0.083	0.072
C	R, P, MSDE	50	2	0.05	0.12	0.083
D	R, P, MSDE	10	1	0.38	0.56	0.092
E	R, P, MSDE	10	2	0.38	0.63	0.010
F	R, P, MSDE	50	2	0.25	0.67	0.017
G	R, P, MSNM	-50	1	0.05	0.17	0.059
H	R, P, MSNM	0	1	0.05	0.25	0.27
I	R, P, MSNM	-50	2	0.05	0.18	0.067
J	R, P, MSNM	0	2	0.05	0.51	0.17

*setting V-vector cut, R-raster etching, P-plastic, A-acyrlic, MSDE-microsurface deep engraving, MSNM-microsurface non-metallic surface.

A

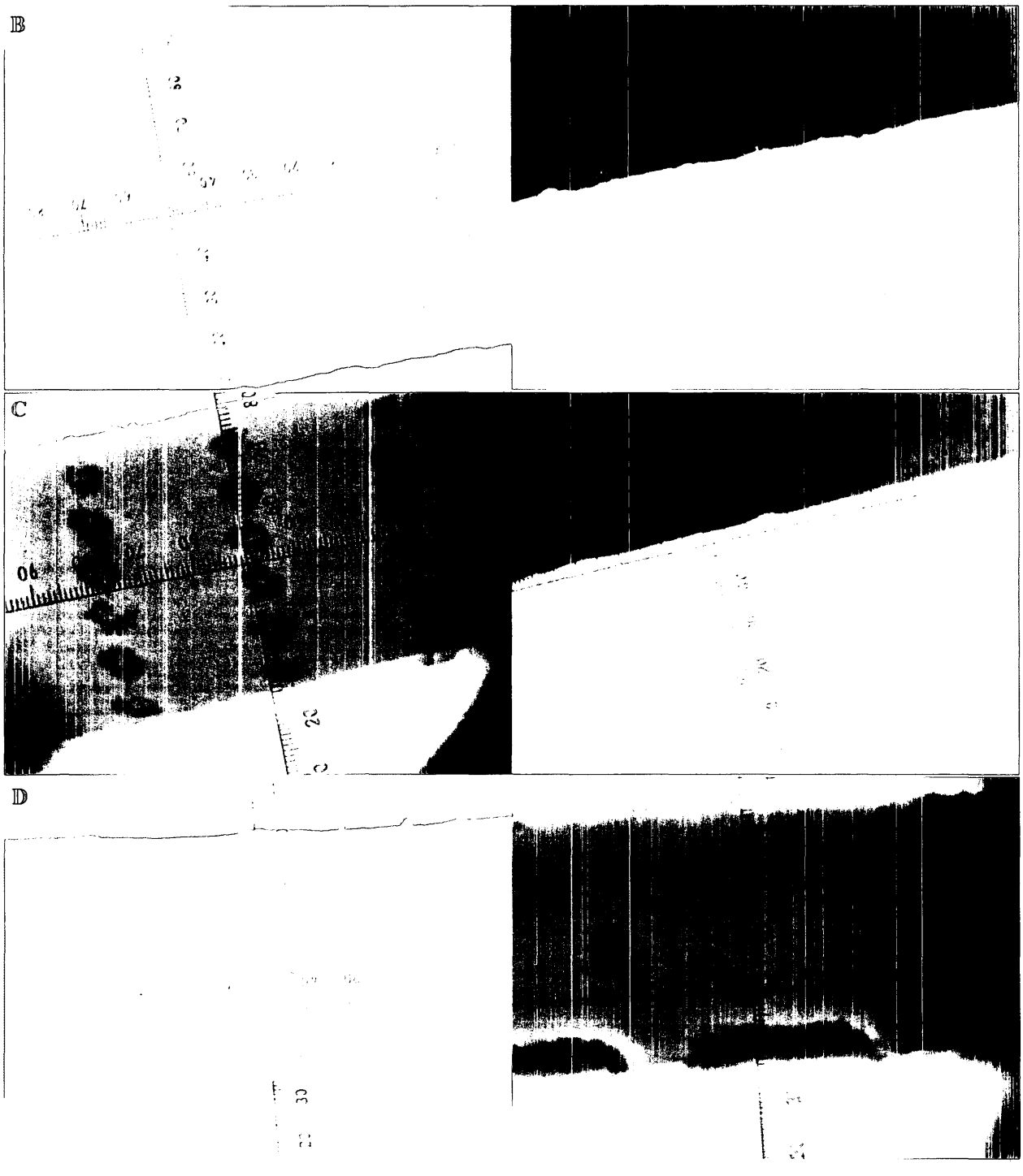
B
C
D

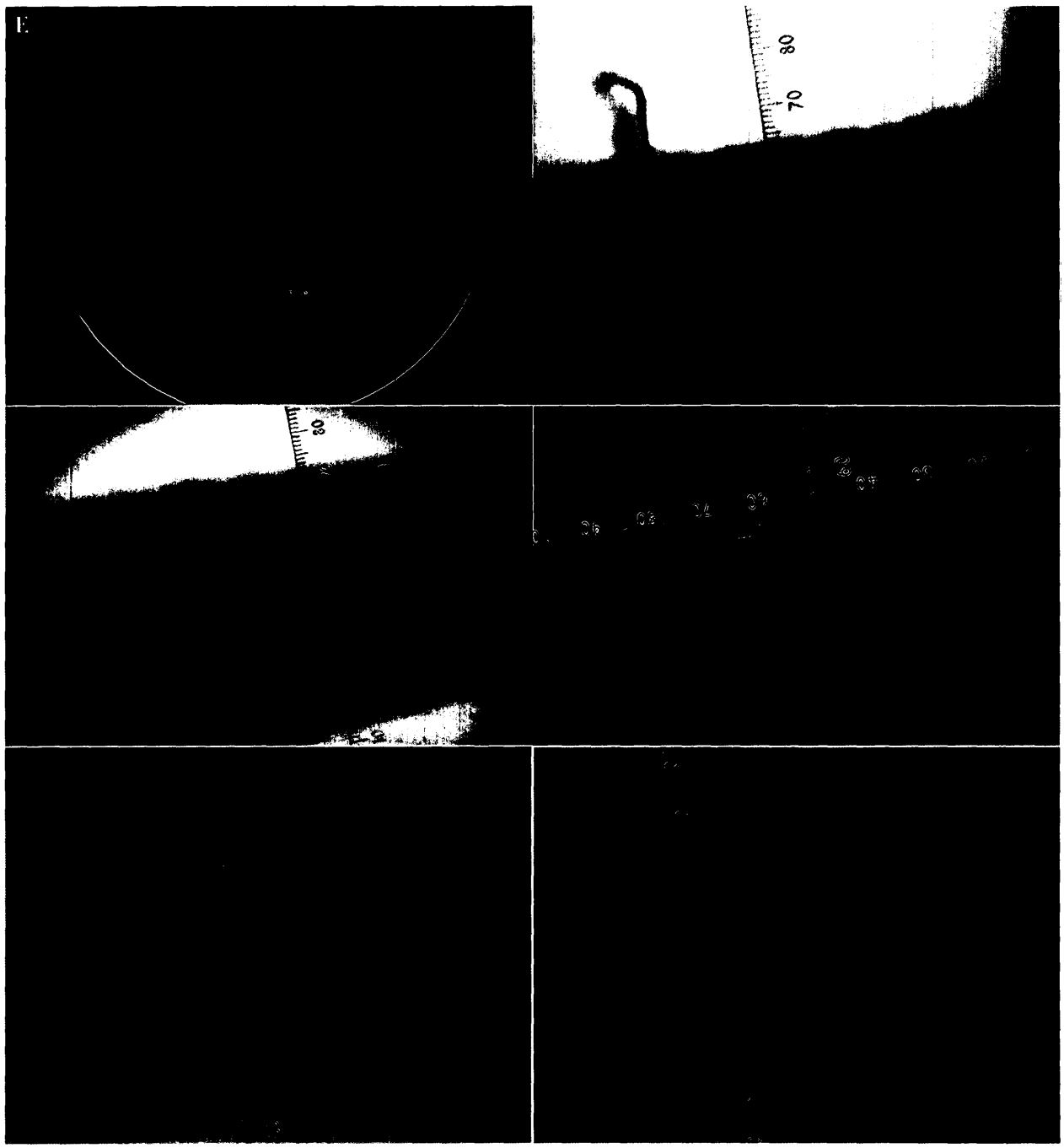

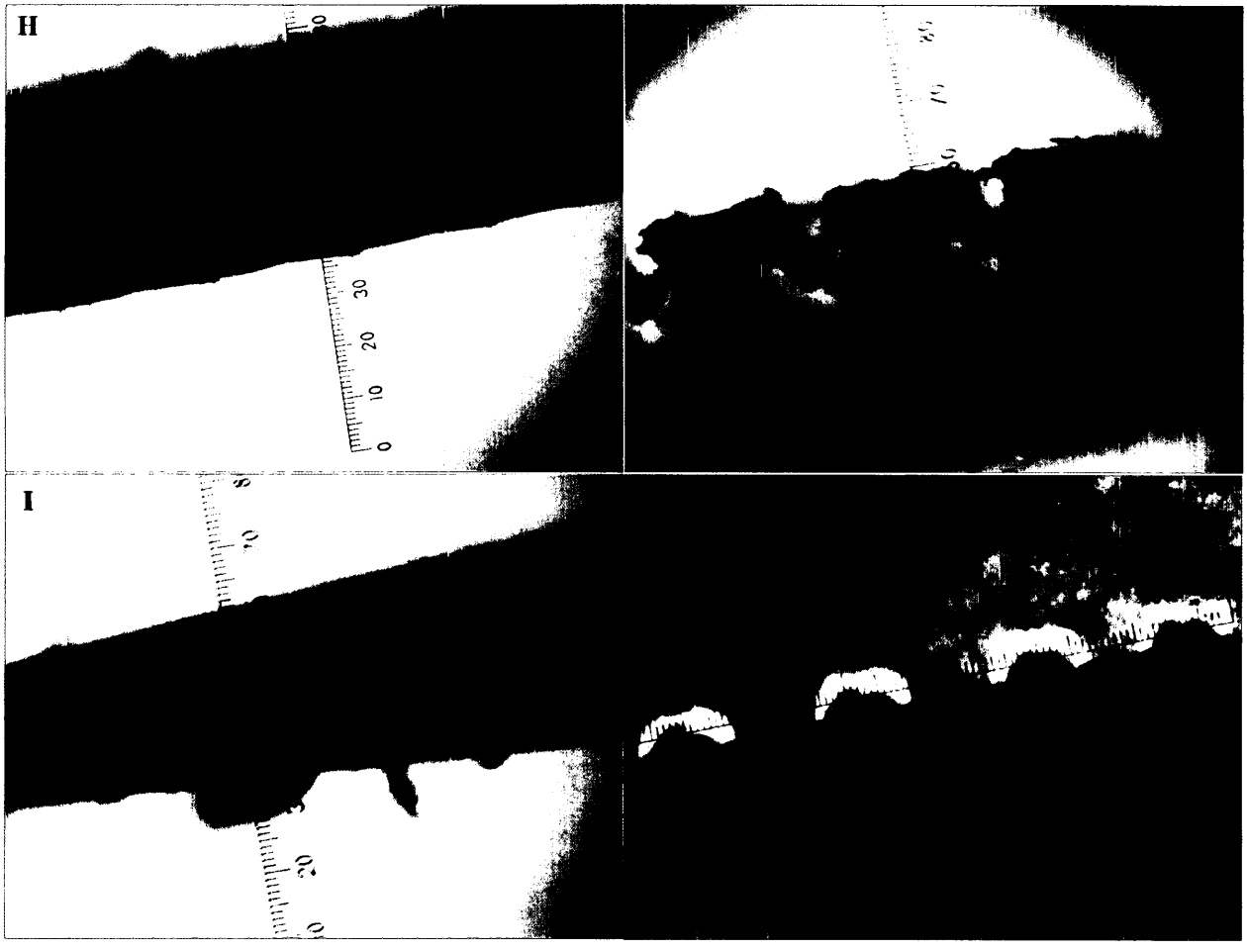
H
0
30
20
10
0
I

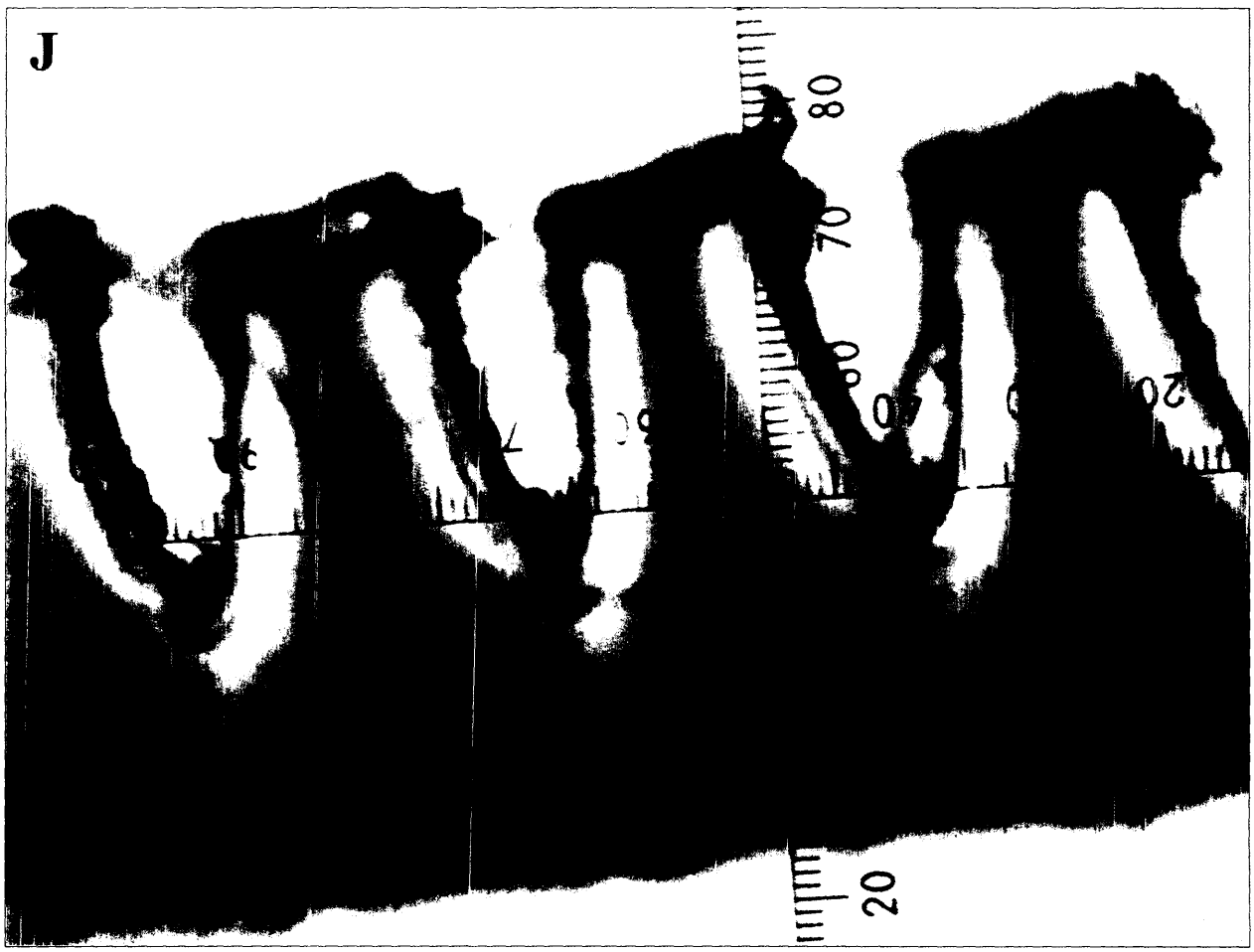

Optical images of further channel etching optimization by laser power variation

Entry	Laser Setting *	Laser Power (%)	Measured Width (mm)	Measured Depth (mm)
A	V, P, MSDE	0	0.28	0.51[a]
B	V, P, MSDE	-25	0.24	0.51
C	V, P, MSDE	-50	0.18	0.37
D	V, P, A	0	0.22	0.49
E	V, P, A	-25	0.26	0.37
F	V, P, A	-50	0.23	0.14
G	V, P, MSNM	0	0.27	0.27
H	V, P, MSNM	-25	0.24	0.13

I	V, P, MSNM	-50	0.16	0.01

*setting V-vector cut, R-raster etching, P-plastic, A-acyrlic, MSDE-microsurface deep engraving, MSNM-microsurface non-metallic surface. All laser cuts were performed using only one pass of the laser beam. The theoretical line width of all cuts according to the drawn line width is 0.05mm. a) A very small amount of PTFE material remains at the trough of the channel, which still holds the structure together.

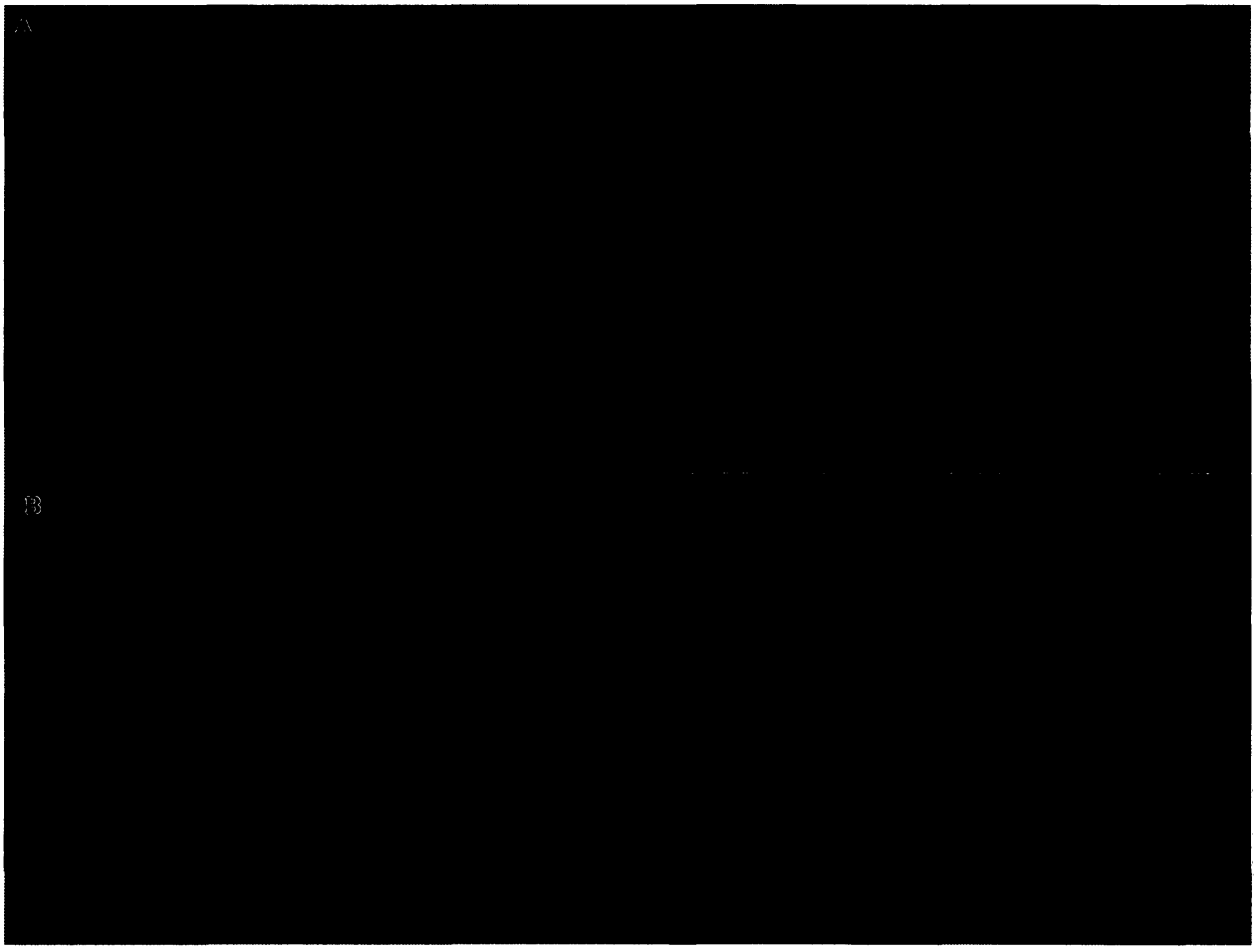

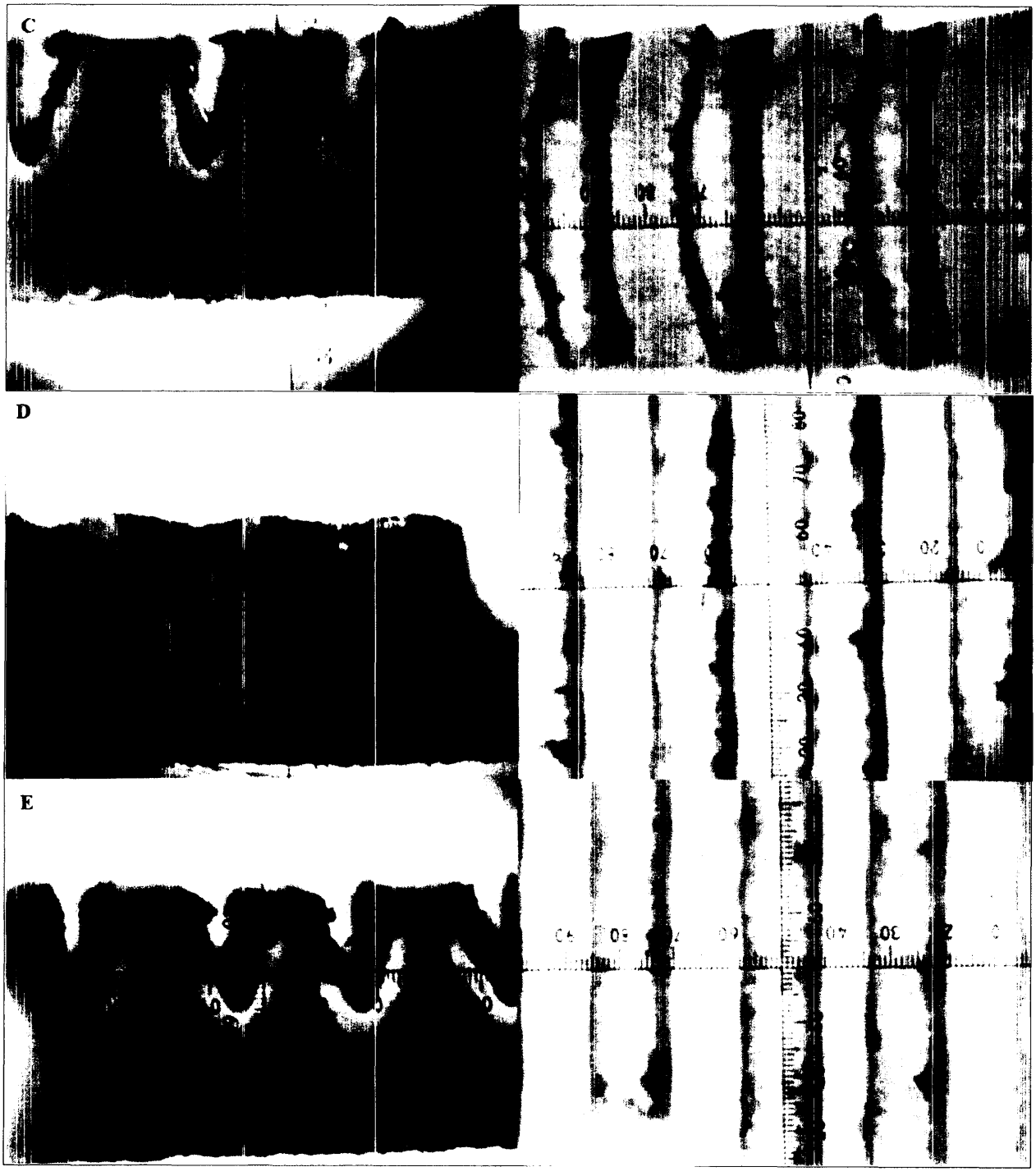
C
D
E

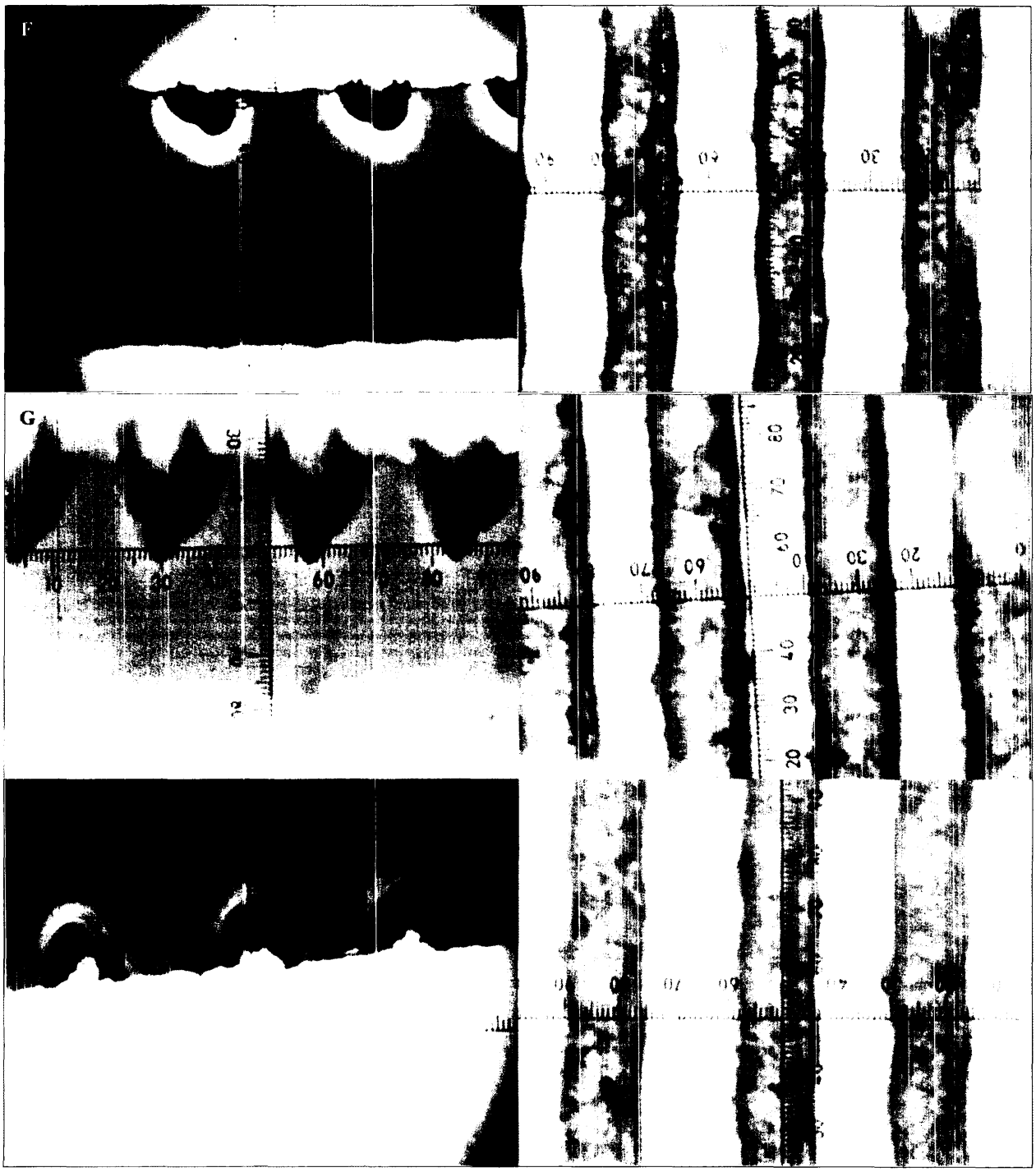
F
G

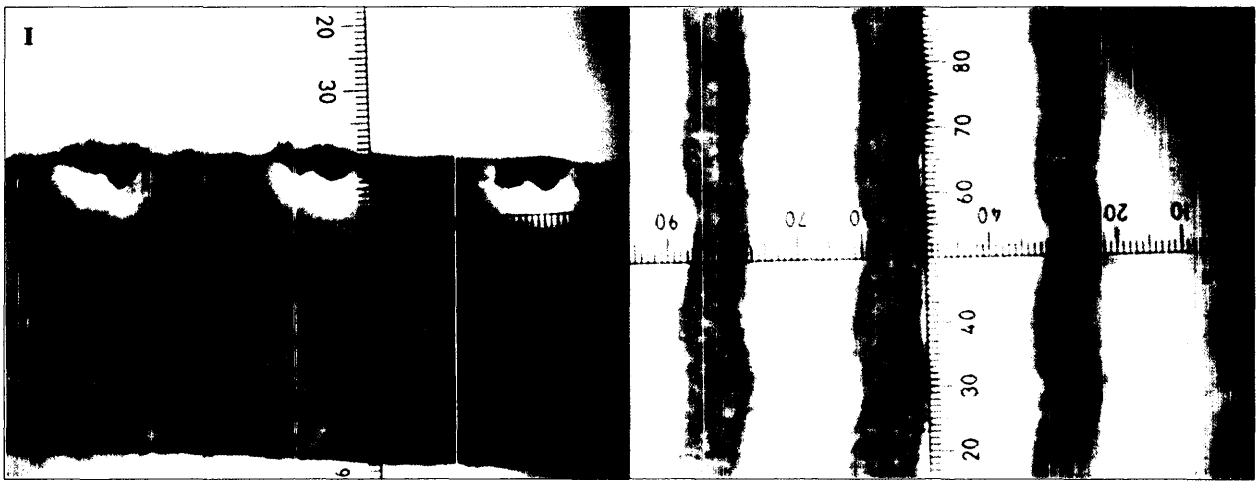
I